DEPARTMENT OF DEFENCE
DEFENCE SCIENCE & TECHNOLOGY ORGANISATION
DSTO

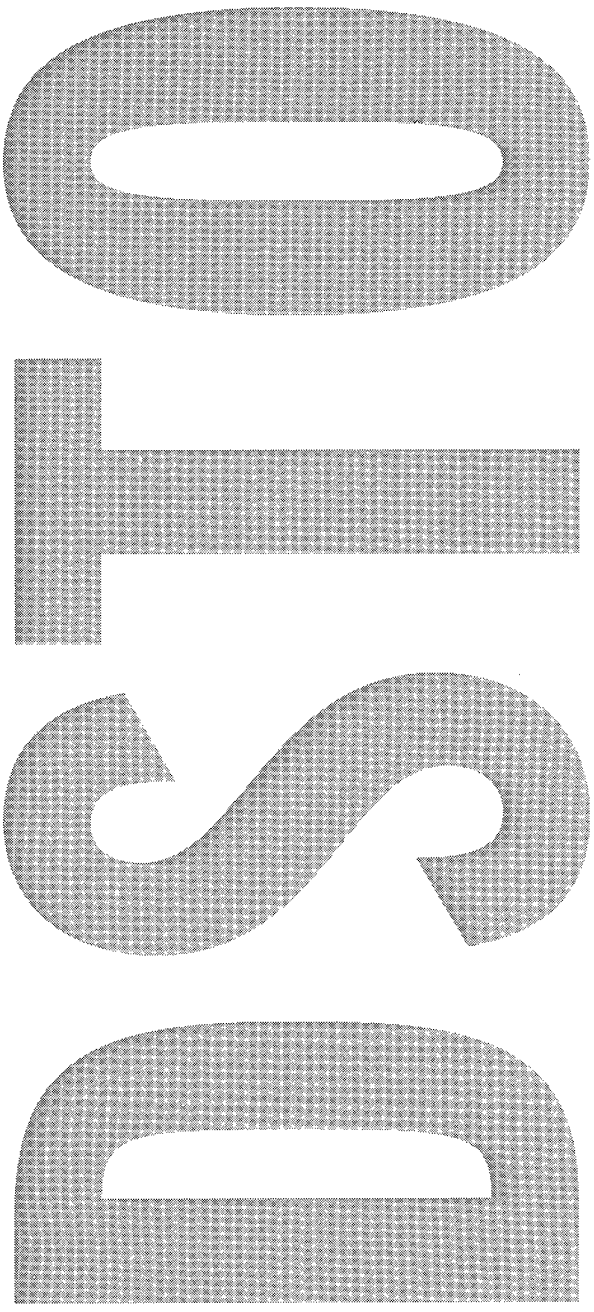

Estimating the Parameters of the K Distribution in the Intensity Domain

Nicholas J. Redding

DSTO-TR-0839

Estimating the Parameters of the K Distribution in the Intensity Domain

Nicholas J. Redding

Surveillance Systems Division
Electronics and Surveillance Research Laboratory

DSTO–TR–0839

ABSTRACT

This paper reviews a number of different moment-based methods for estimating the parameters of the K distribution. The K distribution is a model for the statistics of synthetic aperture radar (SAR) imagery that is formed from the product of two independent distributions, one representing the radar cross-section, and the other representing speckle that is a characteristic of coherent imaging. A method for synthesizing correlated K-distributed random fields is reviewed. Moments of intensity, log intensity and amplitude statistics are used to compute measures which are inverted to give estimates of the mean and order parameters of the K distribution. A method based on the normalized logarithm of intensity is shown to give the best performance, confirming the results of Oliver (1993) and Blacknell (1994). The effect of correlation upon order parameter estimation and its role in the K distribution's underlying component pertaining to the radar cross-section is briefly considered. This work will be used to development target detection algorithms to find targets of interest in SAR imagery.

Published by

DSTO Electronics and Surveillance Research Laboratory
PO Box 1500
Salisbury, South Australia, Australia 5108

Telephone: *(08) 8259 5555*
Facsimile: *(08) 8259 6567*

AR No. 011-015
July, 1999

APPROVED FOR PUBLIC RELEASE

Estimating the Parameters of the K Distribution in the Intensity Domain

EXECUTIVE SUMMARY

An essential first step in the parametric approach to detection is to obtain an adequate model for the statistics of the background process or "clutter" so that it can be distinguished from targets of interest. Targets of interest are then assumed to have a behaviour that is abnormal for the statistics of their local neighbourhood as described by the parametric model. Given an adequate model for these statistics, the next step in detection is to estimate the parameters of the model that best fit a particular neighbourhood. The size of this neighbourhood should be as small as possible so that the probability of it being homogeneous is as large as possible and it is most similar to its center pixels or region of interest. There are countervailing pressures, however — the neighbourhood must also be large enough so that reliable estimates of the parameters are obtained. Consequently, the size of the neighbourhood must be carefully chosen.

The final step in the detection process is to compare the center pixels or region of interest with the best-fitting model for the surrounding region and make a decision regarding the likelihood that these pixels belong to the background or are abnormal for it and so should be considered to be a target of interest. This report is concerned with the first two steps in this detection process: the model for the statistics of synthetic aperture radar (SAR) imagery, and how the model parameters may be estimated from a sample of small size.

In particular, this paper reviews a number of different moment-based methods for estimating the parameters of the K distribution. The K distribution is a model for the statistics of SAR imagery that is formed from the product of two independent distributions, one representing the radar cross-section, and the other representing speckle that is a characteristic of coherent imaging. A method for synthesizing correlated K-distributed random fields is reviewed. Moments of intensity, log intensity and amplitude statistics are used to compute measures which are inverted to give estimates of the mean and order parameters of the K distribution. A method based on the normalized logarithm of intensity is shown to give the best performance, confirming the results of Oliver (1993) and Blacknell (1994). The effect of correlation upon order parameter estimation and its role in the K distribution's underlying component pertaining to the radar cross-section is briefly considered.

This work will be used in the development of model-based target detection algorithms to find targets of interest in SAR imagery. These algorithms will form part of the Analysts' Detection Support System (ADSS) which is designed to reduce the analysts' workload in the Broad Area Aerial Surveillance component of Joint Program 129.

Authors

Nicholas J. Redding
Surveillance Systems Division

Nicholas Redding received a B.E. and Ph.D. in electrical engineering all from the University of Queensland, Brisbane, in 1986 and 1991, respectively. From 1988 he received a Research Scientist Fellowship from the Australian Defence Science and Technology Organisation (DSTO) and then joined DSTO in Adelaide as a Research Scientist after completing his Ph.D. in artificial neural networks in 1991. In 1996 he was appointed as a Senior Research Scientist in the Microwave Radar Division (now Surveillance Systems Division) of DSTO. Since joining DSTO he has applied image processing techniques to the automatic classification of ionospheric data, and more recently researched target detection (both human and algorithmic) in synthetic aperture radar imagery.

Contents

Figures

1 Introduction

An essential first step in the parametric approach to detection is to obtain an adequate model for the statistics of the background process or "clutter" so that it can be distinguished from targets of interest. The targets of interest are assumed to have a behaviour that is abnormal for the statistics of their local neighbourhood as captured by the parametric model. Given an adequate model for these statistics, the next step in detection is to estimate the parameters of the model that best fit a particular neighbourhood. The size of this neighbourhood should be as small as possible so that the probability of it being homogeneous is as large as possible and it is most similar to its center pixels or region of interest. The final step in the detection process is to compare the center pixels or region of interest with the best-fitting model for the surrounding region and make a decision regarding the likelihood that these pixels belong to the background or are abnormal for it and so should be considered to be a target of interest. This report is concerned with the first two steps in this detection process: the model for the statistics of synthetic aperture radar (SAR) imagery and how the model parameters may be estimated from a sample of small size.

In the next section we will consider the K distribution which has been considered as a model for the statistics of SAR imagery. Next, section 3 will look at its correlation properties and section 4 will review a method for simulating a correlated K-distributed random field. Section 5 will review a number of moment-based methods for computing the parameters of the K distribution, which is followed by consideration of parameter estimation in the presence of correlated samples. Finally, section 6 considers the effect of correlation upon the variance of the estimators and section 7 presents the conclusions.

2 Derivation and Properties of the K Distribution

The K distribution can be shown to arise when a gamma-distributed surface cross-section is imaged with coherent radiation [26]. Indeed, the K distribution has been popular for some time as a model of the single-point statistics of high resolution radar [35]. Physically, the K distribution can be justified in the following manner. It arises in the situation where the resolution cell is much larger than the radiation wavelength, and the resolution cell contains N randomly distributed scatters. If the number of scatterers N is distributed according to a negative binomial distribution so that it fluctuates from cell to cell, scattered coherent radiation from the cells would be K distributed [13]. Alternatively, the K distribution may be viewed as a limit process on a two-dimensional random walk of a finite number of steps of fluctuating lengths with the number of steps varying according to the negative binomial distribution [14,15,16]. For our purposes however, it is sufficient to state that when the cross section is gamma distribution (the continuum analogue of the negative binomial distribution), the resulting intensity under coherent radiation is K distributed [22,23,25].

As mentioned above, the K-distribution models the two components that go to make up the radar imagery: the radar cross-section and the noise due to speckle. We will now

see how these two components form the K distribution. We know that the radar cross-section of a cell determines the corresponding pixel's mean intensity and furthermore that it is deterministic and repeatable. However, because small changes in the geometric configuration of the scatterers in the cell change the phase relationships of the scattered radiation and hence the observed intensity, the radar cross section is best considered as a random distribution parameterized by its mean value. Consequently, the radar cross-section is modelled as a gamma-distributed random variable $\boldsymbol{\sigma}$ (for justification, see the references in the previous paragraph) given by the probability density function

$$f_{\boldsymbol{\sigma}}(\sigma) = \frac{1}{\sigma}\left(\frac{\nu\sigma}{\mu}\right)^{\nu}\frac{1}{\Gamma(\nu)}\exp\left(-\frac{\nu\sigma}{\mu}\right) \tag{1}$$

where $\Gamma(\cdot)$ is the gamma function, $\mu = \langle\sigma\rangle$ is the mean, and ν is the order (normally, the gamma distribution is expressed in terms of a scale parameter $\gamma = \mu/\nu$ and shape parameter $\alpha = \nu$). The variance of $\boldsymbol{\sigma}$ is μ^2/ν, so ν is inversely proportional to the variance of the cross section. In the next subsection we will allow for the possibility that the cross section can be correlated from cell to cell, which reflects the correlation properties of the imaged scene.

The observed intensity, the random variable $\mathbf{x}$, is produced by the speckle random process with position dependent mean values given by the radar cross-section at each point. During imaging, an option is available to average a number of independent images of a scene (termed "looks") and this averaging has the effect of reducing the variance of the speckle. If each of the single-look pixels in an L-look resolution cell has the same constant radar cross-section then the L-look amplitude random variable (the square root of the intensity) will be Rayleigh distributed with $2L$ degrees of freedom. However, when the radar cross-section is gamma distributed (1), then the intensity of the multi-look pixels will be K-distributed assuming that speckle and radar cross-sections have very different scales and therefore can be treated separately [28, p. 130]. For L-look SAR imagery [3,29], the conditional probability density function of the intensity $\mathbf{x}$ due to multi-look averaged speckle process is given by

$$f_{\mathbf{x}|\boldsymbol{\sigma}}(x|\sigma) = \frac{1}{x}\left(\frac{Lx}{\sigma}\right)^{L}\frac{1}{\Gamma(L)}\exp\left(-\frac{Lx}{\sigma}\right) \tag{2}$$

so that the probability density function of $\mathbf{x}$ is given by the integral over all possible cross section realizations is

$$f_{\mathbf{x}}(x) = \int_0^{\infty} f_{\mathbf{x}|\boldsymbol{\sigma}}(x|\sigma) f_{\boldsymbol{\sigma}}(\sigma)\, d\sigma. \tag{3}$$

Evaluating this integral gives the K distribution

$$f_{\mathbf{x}}(x) = \frac{2}{x}\left(\frac{L\nu x}{\mu}\right)^{\frac{L+\nu}{2}}\frac{1}{\Gamma(L)\Gamma(\nu)}K_{\nu-L}\left(2\sqrt{\frac{L\nu x}{\mu}}\right) \tag{4}$$

where $K_{\nu-L}(\cdot)$ is a modified Bessel function of the second kind of order $\nu - L$ [36]. Note that it is usually assumed that the speckle is independent from cell to cell because small scale features are uncorrelated at spatially separated locations [31]. Note too that the K

distribution is symmetric in L and ν because the modified Bessel function is even in its order parameter, although non-integer values of L do not have physical meaning.

The integral of (3) makes the above formulation of the K distribution cumbersome to deal with analytically. However, it is possible to formulate the K distribution of (4) by what is termed the *product model.* Let $\mathbf{z}$ denote L-look speckle random variable of mean $\langle \mathbf{z} \rangle = 1$ with probability density function given by

$$f_{\mathbf{z}}(z) = \frac{L^L z^{L-1} e^{-Lz}}{\Gamma(L)}. \tag{5}$$

Then the product of random variables $\mathbf{x} = \boldsymbol{\sigma}\mathbf{z}$ is K distributed with probability density function given by (4), where the random variable $\boldsymbol{\sigma}$ is distributed as before in (1). This can be shown by evaluating the integral for the product of two independent probability density functions [11],

$$f_{\mathbf{x}}(x) = \int_{-\infty}^{\infty} \frac{d\sigma}{|\sigma|} f_{\mathbf{z}}\left(\frac{x}{\sigma}\right) f_{\boldsymbol{\sigma}}(\sigma),$$

using the fact that $\boldsymbol{\sigma} \geqslant 0$.

For this model to be a reasonable one, it is necessary that the speckle and radar cross-section have spatial fluctuations that are very different. As pointed out in [28], the effective point-spread function and sampling of the SAR sensor would in practice not make this the case, particularly in the intensity domain, and so the SAR image is normally resampled so that speckle has little correlation from pixel to pixel. If the contributions are not separable in the sense that multi-looking averages speckle without affecting radar cross-section fluctuations, then the result of multi-looking will not be K-distributed.

The moments of the K distribution always lie between those of the negative exponential distribution and those of the log-normal distribution having the same mean and variance [13, p. 811]. The moments of the K distribution are given by

$$\langle \mathbf{x}^m \rangle = \frac{\mu^m \Gamma(L+m)\Gamma(\nu+m)}{L^m \nu^m \Gamma(L)\Gamma(\nu)}, \tag{6}$$

so that the mean of the K distribution is given by μ, and its variance is

$$\mathrm{var}(\mathbf{x}) = \mu^2 \left(\frac{\nu + L + 1}{L\nu}\right). \tag{7}$$

In the case of small $\nu \ll 1$ (about 0.1 or even smaller), K-distributed random variables are very "spiky". When ν is large (about 10.0 and larger), K-distributed random variables do not exhibit this spikiness.

The K distribution is less sensitive to the parameter ν at large values of ν, and as a consequence, the variance in estimates of ν will increase with ν, even though the estimated probability density function may not visibly vary. This behaviour can be seen in the graphs of figure 1.

Oliver and Quegan [28, pp. 135–138] provide a comparison of four commonly used models for the statistics of SAR imagery and compare them with the K distribution model.

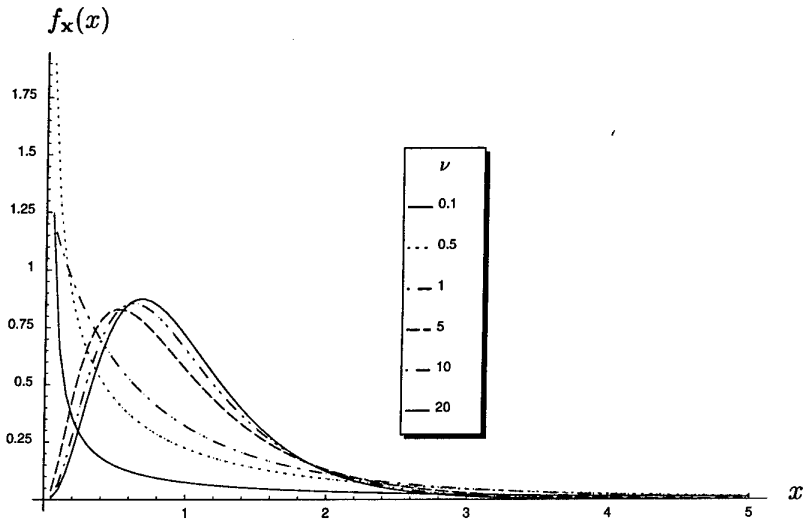

Figure 1: The variability in the shape of the K distribution's probability density function decreases with increasing ν. The probability density functions here are for $L = 4$ and $\mu = 1$.

These models are the log normal, exponential, Weibull and gamma probability density functions. Using homogeneous pieces of SAR imagery of a field and some woodland they examine using the Kolmogorov-Smirnov statistic the probability that the data from each sample follows each of these models after estimating their maximum likelihood parameters. In the case of the field, the observed probability density function had a variance that was lower than that predicted by the speckle model alone so fitting a K distribution proved impossible. Oliver and Quegan state that this would be expected to occur in roughly half the samples taken over regions of constant radar cross-section, and it is reasonable to assume in such circumstances that the region contains a constant radar cross section such that $\nu = \infty$. (This should also be considered in the light of the K distribution's increasing insensitivity to ν as ν increases.) We will observe this behaviour later in this report when we come to moment-based estimators for the order of K-distributed samples. The best fitting distribution was the Weibull with a probability of 0.781, followed by a gamma distribution (0.683), an exponential distribution (0.572) and finally a log normal distribution (6.8×10^{-11}). In the second case of a region of woodland SAR imagery, the goodness of fit was a stark contrast: the K distribution fitted with a probability of 1.000, followed by the Weibull (2.1×10^{-12}), gamma (1.4×10^{-54}), log normal (6.6×10^{-106}) and exponential distributions (0.0), according to the Kolmogorov-Smirnov statistic.

3 Correlation Properties

As mentioned above, the radar back-scatter is commonly correlated from one resolution cell to the next, but the speckle is usually modelled as being uncorrelated across cells. We can use the product model to determine the correlation function of the resulting K distribution in terms of the correlation coefficient of the radar cross-section $\rho_\sigma(r)$ at lag r

[20]. To simplify notation for the time being we will assume that we are dealing with a one-dimensional array of random variables $\mathbf{x}_i$ so that the lag r is a scalar and we will mostly drop the r for convenience. If $\rho_{\mathbf{x}}(r)$ denotes the correlation coefficient of random variable $\mathbf{x}$ at lag r, then (ignoring the separate indices for directions on the two-dimensional grid of the image)

$$\begin{aligned}\rho_{\mathbf{x}}(r) &= \frac{\mathrm{cov}(x_i, x_{i+r})}{\mathrm{var}(x_i)} \\ &= \frac{\langle x_i x_{i+r}\rangle - \langle x_i\rangle^2}{\langle x_i^2\rangle - \langle x_i\rangle^2}.\end{aligned} \tag{8}$$

After substituting the product model and the moments of the two probability density functions in (1) and (5), and using that $\mathbf{z}$ and $\boldsymbol{\sigma}$ are independent of each other as well as that the autocorrelation sequence of the speckle random variable $\mathbf{z}$ is a Kronecker delta function δ_r, we obtain

$$\rho_{\mathbf{x}}(r) = \frac{L}{\nu + L + 1}\rho_{\boldsymbol{\sigma}}(r) + \delta_r \frac{\nu + 1}{\nu + L + 1}. \tag{9}$$

Note that the correlation coefficient $\rho_{\mathbf{x}}(r)$ in (9) matches the single look case presented in [20] when the substitution $L = 1$ is made. It can be seen that the resulting correlation coefficient is composed of a spike at the origin, due to the presence of uncorrelated speckle, and the scaled correlation coefficient due to the correlated cross-section random variable.

Oliver [25] has shown that sometimes the correlation properties of the textures in SAR imagery can be captured using a negative exponential model (along each axis) for the autocorrelation function (ACF) of the radar cross-section $\boldsymbol{\sigma}$. The ACF of $\boldsymbol{\sigma}$ along one axis would thus be given by

$$\rho_{\boldsymbol{\sigma}}(r) = \exp\left(-\frac{r}{\tau}\right). \tag{10}$$

The correlation length, determined by the decay rate τ of this negative exponential model, then provides a single convenient quantity to describe the correlation properties. (Note that the correlation properties of SAR imagery are anisotropic, so two correlation lengths would really be required for the two dimensional field. This is easy to appreciate when one considers that the shadows of trees always fall on the side opposite the sensor.)

The negative exponential model for the ACF arises from a Fokker-Planck rate equation used to model the radar cross-section [15,24,28]. This rate equation is the continuum analogue of a population model with birth, death and migration. The solution of the rate equation yields a gamma-distributed radar cross-section σ, with the correlation coefficient given by (10) and $1/\tau$ the migration rate. Therefore there is some justification for using a negative exponential ACF in conjunction with the gamma-distributed radar cross-section model.

Lombardo and Oliver [20] have shown that it is more accurate to derive the correlation length in the log domain (*i.e.* logarithm of the intensity). This would also be more convenient considering that the imagery is typically quantized to 8 bits after a log transformation. The relationship between the correlation coefficients $\rho_{\boldsymbol{\sigma}}$ in the intensity domain

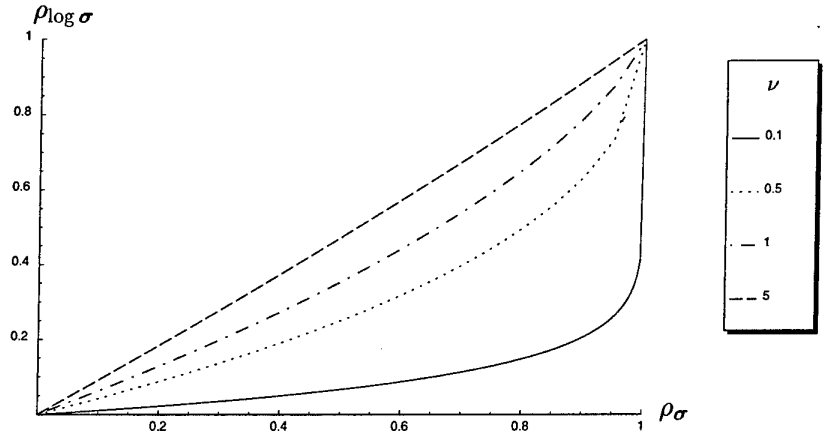

Figure 2: The mapping between the correlation coefficients ρ_σ and $\rho_{\log\sigma}$ for $\nu = 0.1, 0.5, 1, 5$ from (11).

and $\rho_{\log\sigma}$ in the log domain is given by the expression [20]

$$\rho_{\log\sigma} = \frac{(1-\rho_\sigma)^\nu}{\psi^{(1)}(\nu)} \sum_{k=0}^{\infty} \frac{\rho_\sigma^k}{k!} \frac{\Gamma(k+\nu)}{\Gamma(\nu)} \left(\psi^{(0)}(k+\nu) - \psi^{(0)}(\nu) + \log(1-\rho_\sigma)\right)^2 \tag{11}$$

where $\psi^{(0)}(\cdot)$ and $\psi^{(1)}(\cdot)$ are the digamma and trigamma functions, respectively. The curves in figure 2 indicate this relationship. The decorrelating effect of the log transformation for smaller values of ν can clearly be seen. Figure 3 is a plot of the effect that the log transformation has on the exponential ACF, and this effect is quite pronounced for small values of ν. In the log domain, the correlation coefficient of the random variable $\log \mathbf{x}$ is given by

$$\begin{aligned} \rho_{\log\mathbf{x}}(r) &= \frac{\operatorname{cov}(\log x_i, \log x_{i+r})}{\operatorname{var}(\log x_i)} \\ &= \frac{\langle \log x_i \log x_{i+r} \rangle - \langle \log x_i \rangle^2}{\langle \log^2 x_i \rangle - \langle \log x_i \rangle^2} \end{aligned} \tag{12}$$

which when evaluated gives that

$$\rho_{\log\mathbf{x}}(r) = \frac{\psi^{(1)}(\nu)}{\psi^{(1)}(\nu) + \psi^{(1)}(L)} \rho_{\log\sigma}(r) + \delta_r \frac{\psi^{(1)}(L)}{\psi^{(1)}(\nu) + \psi^{(1)}(L)} \tag{13}$$

(only the special case of $L = 1$ is presented in [20]). It can be seen that the two-component structure of the correlation has been preserved in the log domain: there is again a spike at the origin, and a weighted lag-dependent term due to the underlying cross-section. Therefore, as a consequence of the spike in (13) and the relationship between $\rho_{\log\sigma}$ and ρ_σ in (11), very little of the correlation structure of the underlying radar cross-section will be visible from the random variable $\mathbf{x}$ in the logarithm domain. This can be seen in figure 4 where the ACF of $\log \mathbf{x}$ is plotted using (11) and (13), when the radar cross-section has a negative exponential ACF.

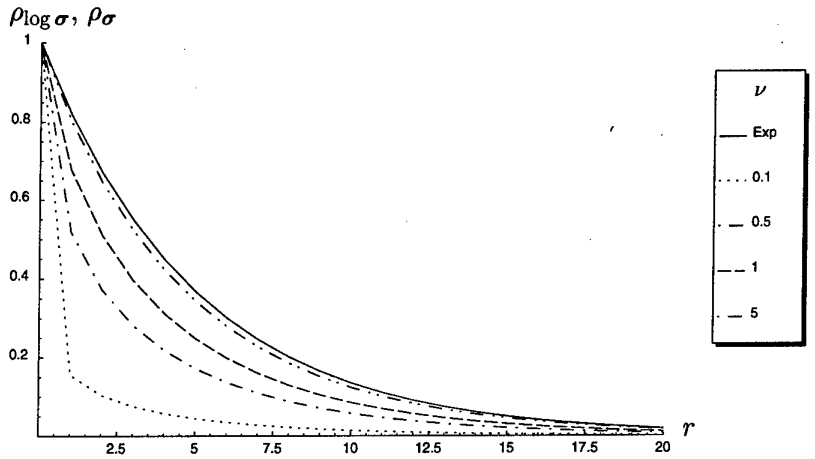

Figure 3: The effect of mapping to the log domain upon a negative exponential ACF can be seen in this plot of the correlation in the log domain $\rho_{\log\sigma}$ from (11) versus the lag r for each of $\nu = 0.1, 0.5, 1, 5$. The outer-most curve is a plot of the correlation ρ_σ versus lag r for a negative exponential ACF for comparison with $\tau = 5$.

4 Simulating Correlated K-Distributed Random Fields

To be able to empirically test the performance of the estimators for the parameters of the K distribution when the samples are correlated as discussed later in this report, it is necessary to be able to generate imagery of known statistics with a range of correlation structures. The method used here to do this firstly computes a two-dimensional Gaussian random field with a desired ACF using the method of Dietrich and Newsam presented in [7,8]. It proceeds as follows.

Let us assume that the Gaussian random field is to have an ACF given by $\rho_g(\tau;\mathbf{r})$ with parameter τ (which could be a vector) and lag variable $\mathbf{r} \in \{0, M-1\} \times \{0, N-1\}$. We will discuss later how to determine $\rho_g(\tau;\mathbf{r})$ from the desired ACF $\rho_\sigma(\mathbf{r})$ of the K-distributed field.

Let the size of the random field we wish to generate be $M \times N$. To begin the method, firstly generate a two-dimensional array $\mathbf{s}$ of size $(M+1) \times (N+1)$ from $\rho_g(\tau;\mathbf{r})$ such that

$$[\mathbf{s}]_{i,j} = \rho_g(\tau;\mathbf{r} = \{i,j\}), \qquad i = 0,\ldots,M \qquad j = 0,\ldots,N.$$

Periodically extend $\mathbf{s}$ to form $\mathbf{s}'$ which is $2M \times 2N$ so that any row i of s given by $[\rho_{i,0},\ldots,\rho_{i,N}]$ becomes $[\rho_{i,0},\ldots,\rho_{i,N},\rho_{i,N-1},\ldots,\rho_{i,1}]$ and similarly for any column i (with the order of indices reversed). If the ACF does not have horizontal and vertical lines of symmetry this procedure is incorrect. In such cases much more complicated steps are necessary here [6,8].

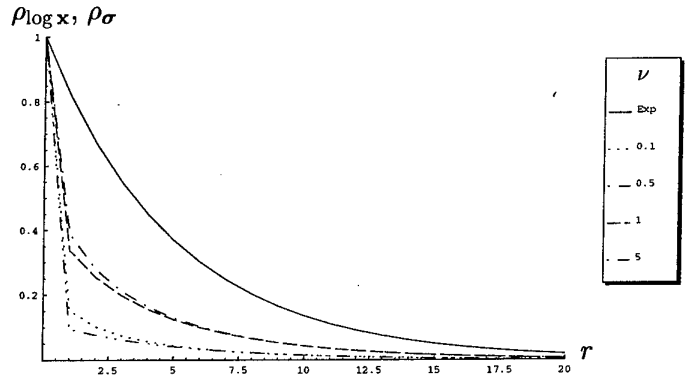

(a) $L = 1$

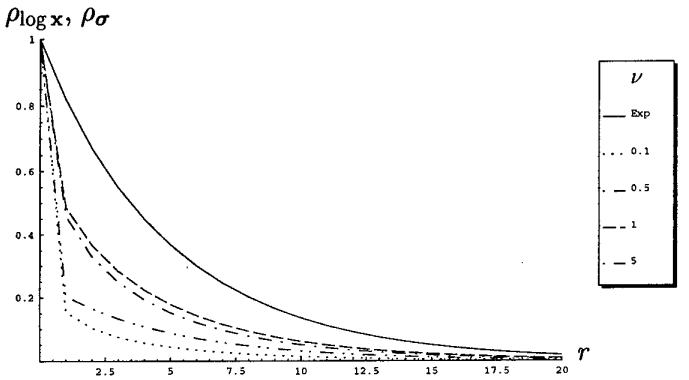

(b) $L = 2$

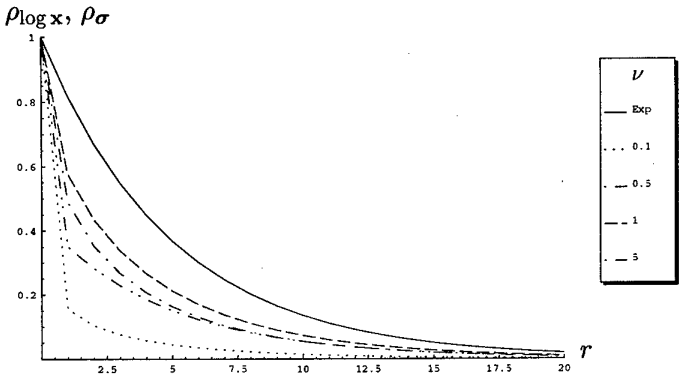

(c) $L = 4$

Figure 4: The effect of mapping to the log domain of an intensity random variable $\mathbf{x}$ *with an underlying radar cross-section* $\boldsymbol{\sigma}$ *which is correlated with a negative exponential ACF* ($\tau = 5$). *The correlation in the log domain* $\rho_{\log \mathbf{x}}$ *from (13) is plotted against lag* r *for each of* $\nu = 0.1, 0.5, 1, 5$. *The outer-most curve is a plot of the correlation* $\rho_{\boldsymbol{\sigma}}$ *versus lag* r *for a negative exponential ACF for comparison with* $\tau = 5$.

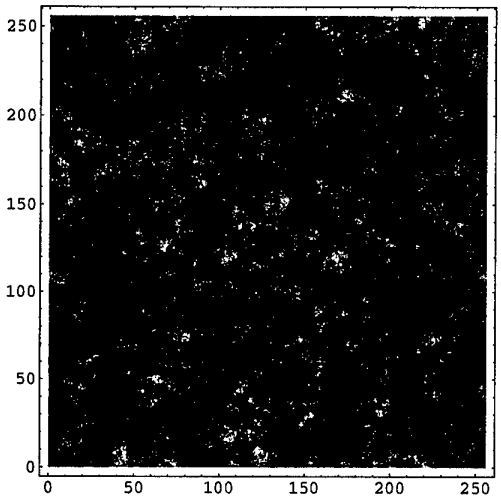

Figure 5: A realization of a correlated Gaussian random field with ACF given by (14) with $\tau = 4$.

Take the discrete Fourier transform of $\sqrt{4MN}\mathbf{s}'$ to give $\tilde{\mathbf{s}}'$,

$$\tilde{\mathbf{s}}' = \mathcal{F}\{\mathbf{s}'\} = \frac{1}{\sqrt{4MN}} \sum_{k=0}^{2M-1} \sum_{l=0}^{2N-1} [\mathbf{s}']_{k,l} e^{\frac{2\pi\imath(k-1)(s-1)}{2M}} e^{\frac{2\pi\imath(l-1)(t-1)}{2N}}.$$

Set any negative elements of $\tilde{\mathbf{s}}'$ to zero (these will normally be due to precision errors for large classes of ACFs [6]) and take the square root (element by element) of the result to obtain $\tilde{\mathbf{s}}_{\frac{1}{2}}$. Next, generate a $2M \times 2N$ two-dimensional array $\boldsymbol{\varepsilon}$ of independently and identically distributed (iid) complex Gaussian random variables of zero mean and variance 1. Compute the discrete Fourier transform of the element by element product (denoted by $\otimes$) of $\tilde{\mathbf{s}}_{\frac{1}{2}}$ and $\boldsymbol{\varepsilon}$

$$\mathbf{e} = \mathcal{F}\{\tilde{\mathbf{s}}_{\frac{1}{2}} \otimes \boldsymbol{\varepsilon}\}$$

and the real and imaginary components of the upper left-hand $M \times N$ subarray of $\mathbf{e}$, denoted by $\mathbf{e}_s$, will be Gaussian with the desired ACF. Figure 5 shows an example of such a realization with Exponential ACF given by

$$\rho_g(\tau; \mathbf{r} = \{j,k\}) = e^{-\sqrt{j^2+k^2}/\tau} \tag{14}$$

where $\tau = 4$.

The next step is to realize the gamma-distributed random variables $\boldsymbol{\sigma}$ of the radar cross-section from realizations of the Gaussian distributed random fields $\mathbf{e}_{si}$, $i = 1, \ldots, n$, generated above. The random array $\boldsymbol{\Sigma}$ of random variables $\boldsymbol{\sigma}$ can be realized by

$$\boldsymbol{\Sigma} = \sum_{i=1}^{n} \mathbf{e}_{si}^2$$

which gives a gamma distribution with order $\nu = n/2$ and mean $\mu = n$ by (1) (in fact, $\boldsymbol{\Sigma}$ is Chi-squared distributed with n degrees of freedom). Figure 6 shows one realization of a correlated gamma-distributed field that results from this process.

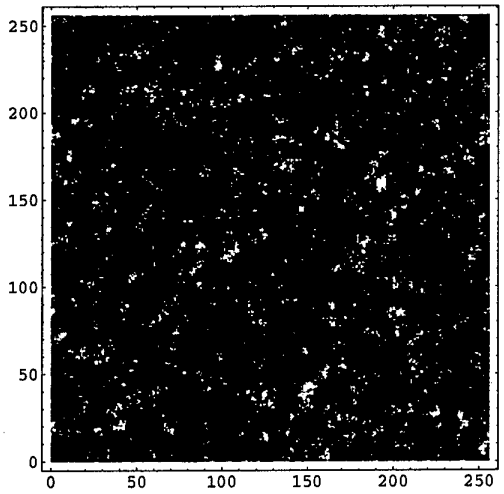

Figure 6: A realization of a correlated gamma distributed random field of $\nu = 2.5$ with the $n = 5$ underlying Gaussians having ACF given by (14) with $\tau = 4$.

The relationship between the correlation coefficients of the gamma and Gaussian random variables used to form them is given by the square of ρ_g [5]. This can be shown in the following manner. From [11, p. 160], the probability density function of a bivariate normal distribution is given by

$$f_{\mathbf{xy}}(x,y) = \frac{1}{2\pi}\frac{1}{\sqrt{1-\rho_g^2}}\exp\left[-\frac{(x^2-2\rho_g xy+y^2)}{2(1-\rho_g^2)}\right] \tag{15}$$

where the correlation between $\mathbf{x}$ and $\mathbf{y}$ is given by

$$\langle \mathbf{xy} \rangle = \rho_g.$$

Let two new random variables be formed by

$$\mathbf{u} = \sum_{i=1}^{n} \mathbf{x}_i^2 \qquad \text{and} \qquad \mathbf{v} = \sum_{i=1}^{n} \mathbf{y}_i^2$$

where the random variables $\mathbf{x}_i$ and $\mathbf{y}_i$ obey (15) and are independent for varying i. Then $\mathbf{u}$ and $\mathbf{v}$ will be gamma distributed according to (1) with $\nu = n/2$ and $\mu = n$. Using laws of expectation it is reasonably straight forward to show that the correlation of $\mathbf{u}$ and $\mathbf{v}$ is given by

$$\langle \mathbf{uv} \rangle = 4\nu(\rho_g^2 + \nu) \tag{16}$$

confirming [2], and that the correlation coefficient of the resulting gamma-distributed radar cross-section is given by

$$\rho_\sigma = \rho_g^2. \tag{17}$$

Armstrong and Griffiths [2] showed that the bivariate gamma probability density function for the random variables $\mathbf{u}$ and $\mathbf{v}$ is given by

$$f_{\mathbf{uv}}(u,v) = \frac{1}{2^{\nu+1}\rho_g^{\nu-1}(1-\rho_g^2)\Gamma(\nu)}(uv)^{(\nu-1)/2}\exp\left[-\left(\frac{u+v}{2(1-\rho_g^2)}\right)\right] I_{\nu-1}\left[\frac{\rho_g\sqrt{uv}}{1-\rho_g^2}\right], \quad (18)$$

where $I_k(\cdot)$ is a modified bessel function of the first kind of order k. They then state that the joint moments of $\mathbf{u}$ and $\mathbf{v}$ are given by

$$\langle(\mathbf{uv})^m\rangle = \frac{2^{2m}(1-\rho_g^2)^{\nu+2m}}{\Gamma(\nu)}\sum_{i=0}^{\infty}\rho_g^{2i}\frac{[\Gamma(\nu+i+m)]^2}{\Gamma(i+1)\Gamma(\nu+i)}, \quad (19)$$

which can be simplified [1,10] to

$$= 4^m(1-\rho_g^2)^{2m+\nu}\frac{[\Gamma(m+\nu)]^2}{[\Gamma(\nu)]^2}\,{}_2F_1(m+\nu,m+\nu,\nu,\rho_g^2), \quad (20)$$

where ${}_2F_1(\cdot)$ is the Gaussian hypergeometric function. In the special case of $m=1$, this simplifies to (16) above.[1]

To obtain non-half integral values of order ν', a nonlinear transformation can be applied to the elements of $\mathbf{\Sigma}$, which in the simplest case of $n=2$ is given by [2]

$$\boldsymbol{\sigma}_{ij} = -2\log\left[1-\frac{1}{\Gamma(\nu')}\gamma\left(\nu',\frac{\nu'\boldsymbol{\sigma}'_{ij}}{\mu'}\right)\right] \quad (23)$$

where $[\mathbf{\Sigma}]_{i,j} = \boldsymbol{\sigma}_{ij}$, the elements of the transformed $\mathbf{\Sigma}'$ with desired order ν' and mean μ' are given by $[\mathbf{\Sigma}']_{i,j} = \boldsymbol{\sigma}'_{ij}$, and γ is the incomplete gamma function. It was observed through simulation that the random variables that result from (23) obey the correlation relationship given in (17) and joint probability density function in (18) [2], although this was not proven. Armstrong and Griffiths were not able to determine analytically the effect of (23) on the resulting correlation, but state that (19) and (20) are still valid from simulation.

The last stage in producing the correlated K-distributed random field is to multiply each element of $\mathbf{\Sigma}'$ by an iid random variable $\mathbf{z}$ with probability density function given by (5), *i.e.* gamma distributed with mean of 1 and order parameter L (the number of looks). Figure 7 shows a realization of the resulting K-distributed random field.

[1]The relationship between the correlation coefficient ρ_g of the underlying Gaussian-distributed random variables and ρ_σ, the correlation coefficient of the gamma-distributed random variables is given in [28, p. 147] as

$$\rho_\sigma = \nu\left\{(1+\rho_g^2)^{\nu+2}\,{}_2F_1(1+\nu,1+\nu,\nu,\rho_g^2)-1\right\}. \quad (21)$$

This expression is incorrect — the first addition occurring in the term $(1+\rho_g^2)$ should be a subtraction. This can be seen by observing that (21) simplifies to

$$\rho_\sigma = \frac{(1+\rho_g^2)^{2+\nu}}{(1-\rho_g^2)^{2+\nu}}(\rho_g^2+\nu)-\nu, \quad (22)$$

which after correcting the sign gives the expression in (17).

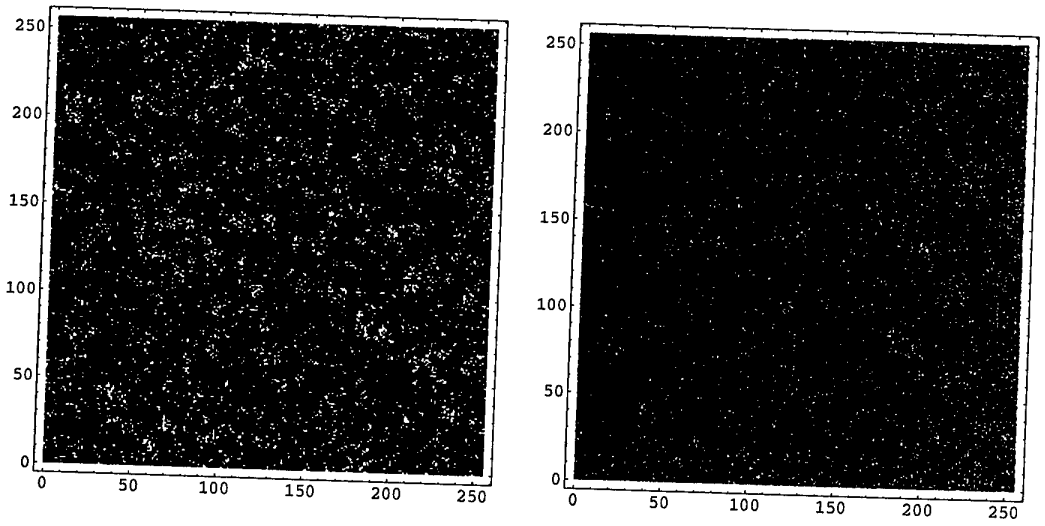

(a) intensity domain

(b) log intensity domain

Figure 7: A realization of a correlated K-distributed random field in the (a) intensity and (b) log domain, with $L = 2$, $\nu = 2.5$ and the underlying Gaussians having ACF given by (14) with $\tau = 4$.

The method presented above has the drawback that not all possible autocorrelation functions can be implemented by normal means (because of the squaring operation no negative correlation coefficients would normally be possible). Oliver and Quegan [28, section 5.8] review other methods (which all have their problems) for simulating correlated K-distributed random fields, most of which also have this drawback. All methods that resample gamma or negative exponential random processes fail to realize the directional effect of shadowing because of their inability to produce ACFs with negative coefficients. There are two exceptions, however. One is a deterministic approach that models tree position and size [9]. For the second, Blacknell *et al.* [4] suggest transforming correlated Gaussian-distributed random variables directly into the desired correlated Gamma-distributed form thereby avoiding the squaring operation and consequent loss of negative correlations (see also [28, pp. 149–151]). There is however no analytic relationship for the effect of the transform on the correlation.

5 Estimators

5.1 Maximum Likelihood

The maximum likelihood estimate for the parameters θ of a distribution from a vector of random variables $\mathbf{X} = (\mathbf{x}_1, \ldots, \mathbf{x}_n)$ is given by maximizing the likelihood function

$$L_{\mathbf{X}}(\theta) = f_{\mathbf{X}}(x_1, \ldots, x_n : \theta)$$

where $f_{\mathbf{X}}(x_1, \ldots, x_n : \theta)$ is the joint probability density function of $\mathbf{X}$ with θ its parameter vector which may be regarded as a random variable dependent upon the data $x_1, \ldots, x_n$. If $\mathbf{x}_1, \ldots, \mathbf{x}_n$ are independent and their probability density function is given by $f_{\mathbf{x}}(x)$, then the likelihood function becomes

$$L_{\mathbf{X}}(\theta) = \prod_{i=1}^{n} f_{\mathbf{x}_i}(x_i : \theta).$$

For the case of the K distribution, we have that $\theta = (\mu, \nu)$ and the probability density function is given by (4). Note that L, the number of looks, is known *a priori*. Maximizing the likelihood function is equivalent to maximizing the log likelihood function, which for the case of independent samples from a K distribution is

$$\log L_{\mathbf{X}}(\mu, \nu) = \sum_{i=1}^{n} \left(-\log x_i + \frac{1}{2}(L+\nu)(\log L + \log x_i + \log \nu - \log \mu) \right.$$
$$\left. + \log \left(K_{L-\nu} \left(2\sqrt{\frac{L x_i \nu}{\mu}} \right) \right) - \log \Gamma(L) - \log \Gamma(\nu) + \log 2 \right). \quad (24)$$

This maximum likelihood estimate for the parameters μ and ν of the K distribution (24) has no closed form and requires a two-dimensional search for its solution. This is computationally too expensive for the applications of interest. The next least expensive approach is to take local estimates for μ by computing the mean in a window and using a one-dimensional search for ν [12]. However, this is still too expensive computationally, and method of moments based approaches offer a speedier alternative. We consider moment-based methods in the following subsections.

5.2 First Moment Estimate for Mean Parameter

The mean parameter μ of the K distribution can be estimated directly from the data using the first moment or sample mean

$$\hat{\mu} = \frac{1}{n} \sum_{i=1}^{n} x_i \quad (25)$$

and this estimate is unbiased and has normalized variance [3]

$$\frac{\mathrm{var}(\hat{\mu})}{\mu^2} = \frac{\nu + L + 1}{n \nu L} \quad (26)$$

which is simply the variance of the distribution reduced by a factor of n.

Figure 8 plots the histogram of estimated mean values using (25) from 1000 simulations with a range of order ν values and differing sample sizes. It is clear that the estimate is unbiased. By 49 samples, there is a reasonably close degree of clustering around the true mean except for small values of $\nu = 0.1$, which require much larger sample sizes. Note that the effect of multi-looking at a fixed sample size is roughly proportional to an equivalent number of samples with a lesser degree of multi-looking treated independently

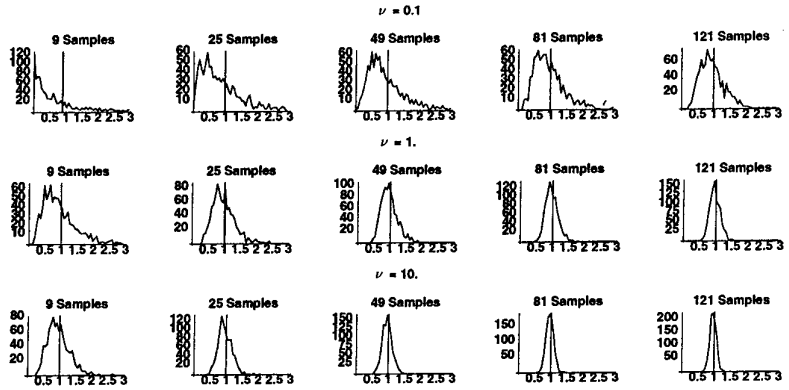

(a) $L = 1$

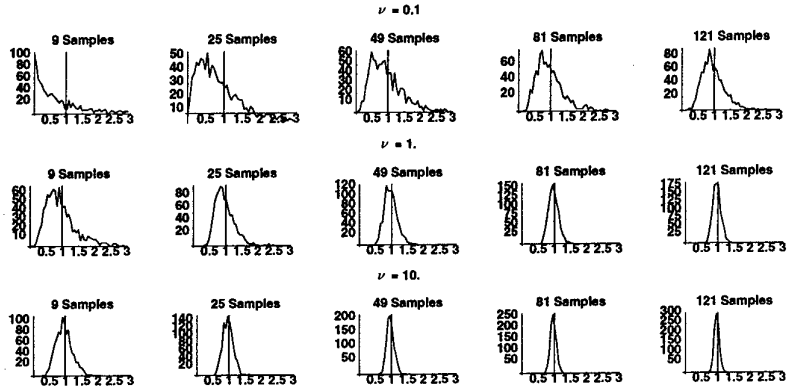

(b) $L = 2$

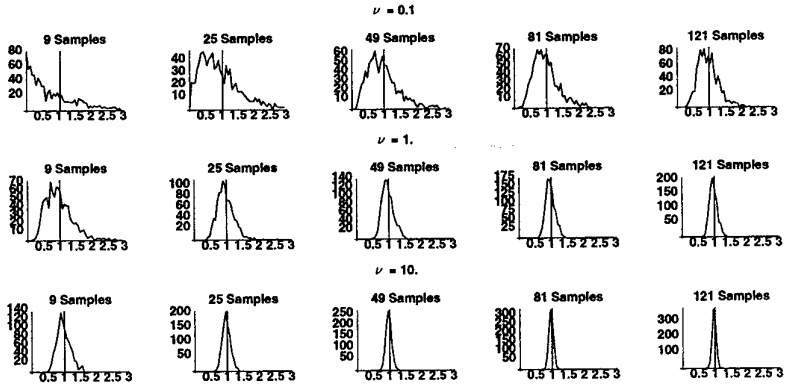

(c) $L = 4$

Figure 8: Plots of the histogram of estimated mean using the sample mean (25) for the cases of $\nu = 0.1$, $\nu = 1.0$ and $\nu = 10.0$ with 9, 25, 49, 81 and 121 samples and $L = 1, 2, 4$ looks calculated over 1000 simulations with $\mu = 1$. The mean of the 1000 mean estimates occurs at the value designated by a vertical line.

for $\nu \geqslant 1.0$ (*e.g.*, two-look with a sample size of 25 is roughly equivalent to single-look with a sample size of 49). Figure 9 plots the normalized variance of the sample mean over the 1000 simulations against the theoretical variance of the sample mean from (26) with which there is a good correspondence. Figure 10 plots the normalized variance of the mean estimate against the actual order parameter of the simulations. The uncertainty in the mean estimates with decreasing ν is clearly visible.

5.3 Maximum Likelihood Using Approximation to K Distribution

Oliver [27] presents a maximum likelihood estimate for the parameters of an approximation to the K distribution. (I will refer to it as the approximate maximum likelihood estimator for convenience.) He derives an approximate probability density function for the K distribution in the limit of large L,

$$f_{\mathbf{x}}(x) \approx f_{\sigma}(x)\left(1+\frac{\nu}{2L}\left(1+\nu-2\frac{x}{\mu}(1+\nu)+\frac{\nu x^2}{\mu^2}\right)\right) \tag{27}$$

and then computes the likelihood function for (27). After differentiating with respect to μ we obtain the maximum likelihood estimate

$$\hat{\mu} \approx \langle x \rangle \left(1+\frac{1}{L}\left(1+\hat{\nu}-\hat{\nu}\frac{\langle x^2 \rangle}{\langle x \rangle^2}\right)\right) \tag{28}$$

to first order in $1/L$. Note that in this case the estimate of μ is not simply given by the sample mean of the data. Then, taking the log of the likelihood function for (27) and differentiating with respect to ν leads to

$$\log\hat{\nu}+1-\log\hat{\mu}-\psi^{(0)}(\hat{\nu}) = -\langle \log x \rangle + \frac{\langle x \rangle}{\hat{\mu}} - \frac{1}{2L}\left(1+2\hat{\nu}-\frac{2}{\hat{\mu}}(1+2\hat{\nu})\langle x \rangle + 2\frac{\hat{\nu}}{\hat{\mu}^2}\langle x^2 \rangle\right). \tag{29}$$

Eliminating $\hat{\mu}$ then gives

$$\log\hat{\nu}-\psi^{(0)}(\hat{\nu})+\frac{\hat{\nu}}{L}\left(\frac{\langle x^2 \rangle}{\langle x \rangle^2}-1\right) = \log\langle x \rangle - \langle \log x \rangle + \frac{1}{2L} \tag{30}$$

to first order in $1/L$. A numerical search is required to determine the estimate $\hat{\nu}$ where the expectations on x are determined from the sample. This is very similar to the moments of logarithm of intensity that we will consider shortly, and it serves to motivate that work.

The approximate bias and variance in the order parameter to first order in $1/L$ and $1/n$ is given by

$$\langle \hat{\nu}-\nu \rangle \approx -\frac{1}{2n(1-\nu\psi^{(1)}(\nu))}\left(1-\frac{1}{L}\left(1+\nu+\frac{1}{1-\nu\psi^{(1)}(\nu)}\right)\right) \tag{31}$$

and

$$\frac{\mathrm{var}(\hat{\nu})}{\nu^2} \approx \frac{\nu\psi^{(1)}(\nu)-1+1/L}{n\nu(1-\nu\psi^{(1)}(\nu))^2} \tag{32}$$

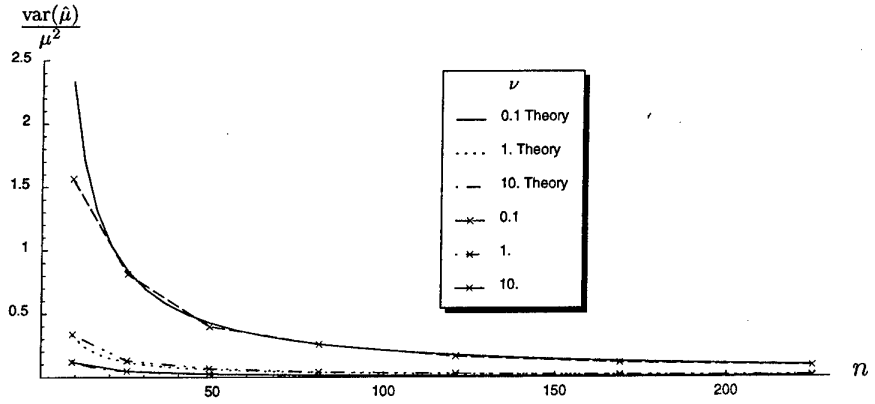

(a) $L = 1$

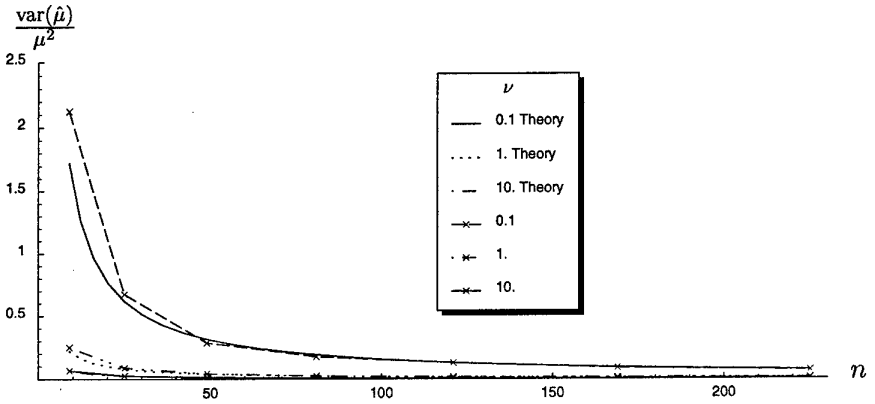

(b) $L = 2$

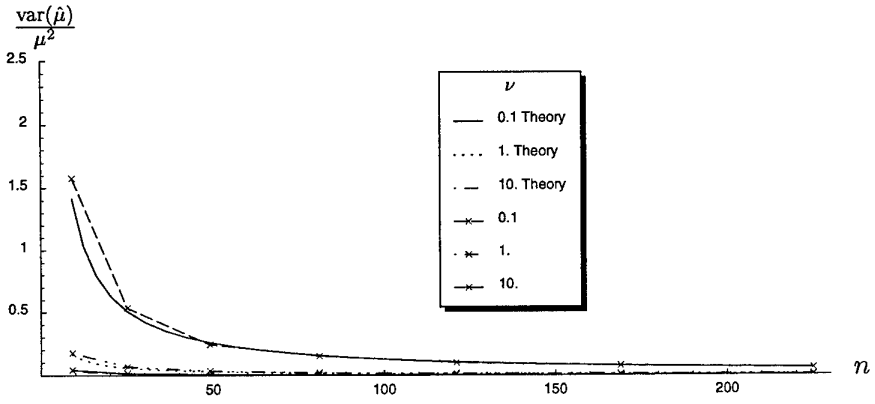

(c) $L = 4$

Figure 9: The normalized variance of the estimated mean using the sample mean (25) as it varies with sample size computed over 1000 simulations with $\mu = 1$ for $L = 1, 2, 4$. The theoretical (26) and calculated values of the normalized variance of the mean estimates are shown for three different values of the order parameter.

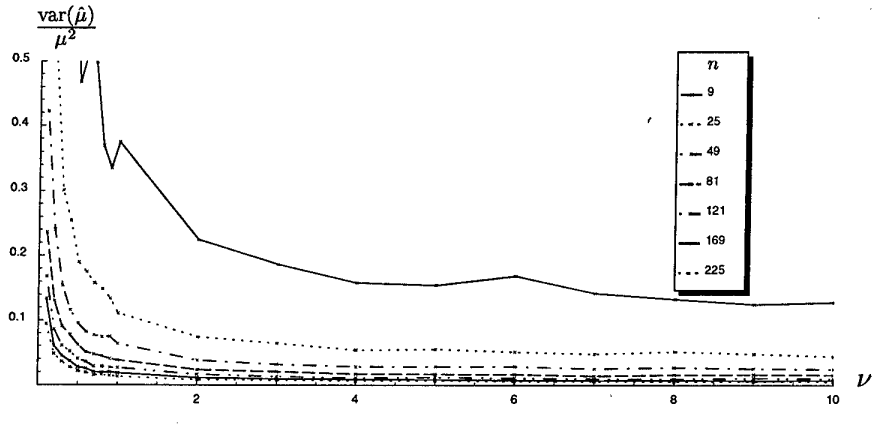

(a) $L = 1$

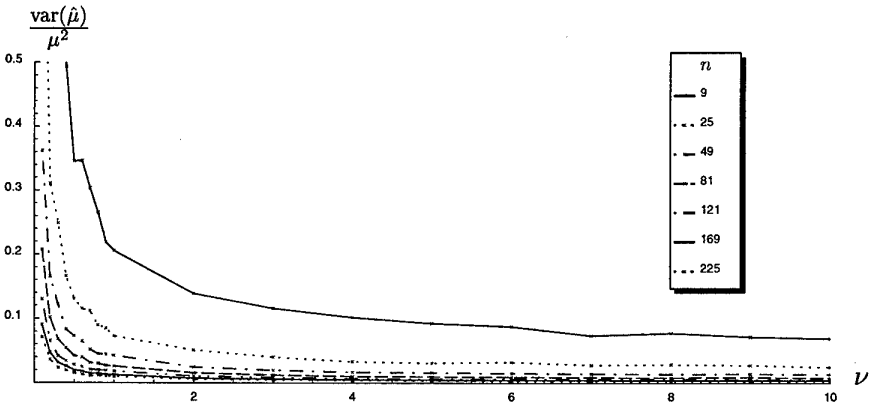

(b) $L = 2$

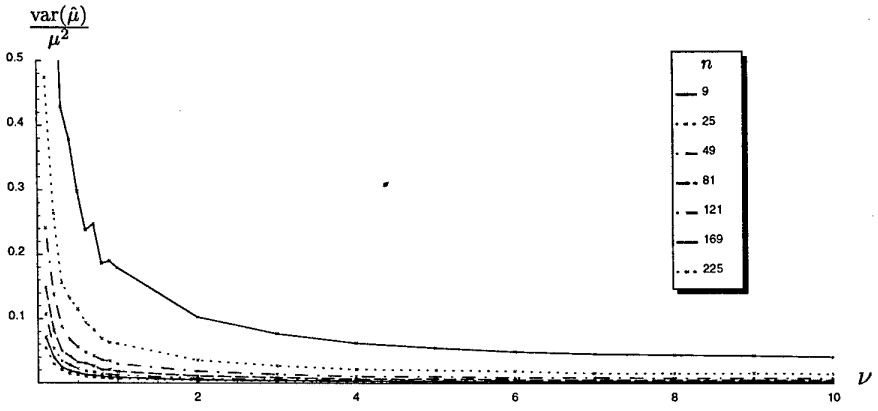

(c) $L = 4$

Figure 10: The normalized variance of the mean estimates using the sample mean (25) as it varies with ν computed over 1000 simulations with $\mu = 1$ for $L = 1, 2, 4$.

respectively. The approximate bias and variance in the mean parameter to first order in $1/L$ and $1/n$ is given by

$$\langle \hat{\mu} - \mu \rangle \approx \frac{\langle x \rangle}{2nL\nu(1 - \nu\psi^{(1)}(\nu))} \quad (33)$$

and

$$\frac{\mathrm{var}(\hat{\mu})}{\mu^2} \approx \frac{\nu + L + 1}{n\nu L} \quad (34)$$

respectively.

Simulations of K-distributed random variables showed that the mean estimate of (28) is unreliable in practise. The variability of the second moment estimate in (28) caused the estimate of the mean to frequently be negative, and this frequency grew with increasing ν, making it unreliable. For this reason, simulation results for this estimator are not reported further here. The discrepancy between the first and second moments of the approximate K distribution in (27) and those of the K distribution in (6) would explain this observation.

Figure 11 plots the histogram of estimated order values using (30) from 1000 simulations for three different values of the order ν and a range of sample sizes and looks. Figure 12 plots the absolute value of the relative bias of the order estimate against the actual order parameter of the simulations. Clearly the order estimate is biased for all but the smallest values of the order parameter in the range. The absolute value of the relative bias is particularly pronounced in the central range of ν (figure 12) and the dip which follows is due to a sign change in the bias $\langle \hat{\nu} - \nu \rangle$, visible in figure 11. Note that increasing the number of looks has the effect of reducing the bias in the lower range of ν. (Note that the approximation was derived for the case of large L.) A vertical line in each of the histograms of figure 11 is used to indicate the 5%-trimmed mean of the order estimates computed over 1000 simulations. In some cases the vertical line is off-scale because of the extremely large values of the order parameter that can sometimes occur in regions where the radar cross-section is close to being constant. As discussed in section 2, these can be interpreted as regions where $\nu = \infty$. The proportion of the simulations in which this occurred is indicated by one minus the number in the upper right hand corner of each histogram of figure 11. This method failed to obtain a positive finite order estimate $\hat{\nu}$ in 20–30% of the cases other than for $\nu = 0.1$, and these cases must be interpreted as $\nu = \infty$ according to the estimator. (The test for interpreting ν as ∞ included: negative values of ν, situations where no value for ν was found in a fixed number of iterations when solving (30), and values of ν that were $> 10^5$.) The predicted relative bias (31) is an extremely poor match (figure 12).

Figure 13 plots the normalized variance of the order parameter estimate computed during the 1000 simulations for each sample size and number of looks against the theoretical variance of the order from (49). The predicted normalized variance is a poor match. Figure 14 plots the normalized variance of the order estimate against the actual order parameter of the simulations. The normalized variance is very large across much of the range of ν, but the decrease that is apparent for large ν must be offset against the large relative bias in this range (figure 12).

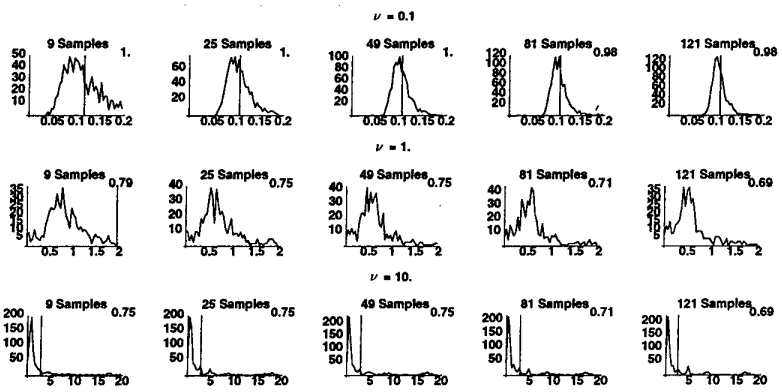

(a) $L = 1$

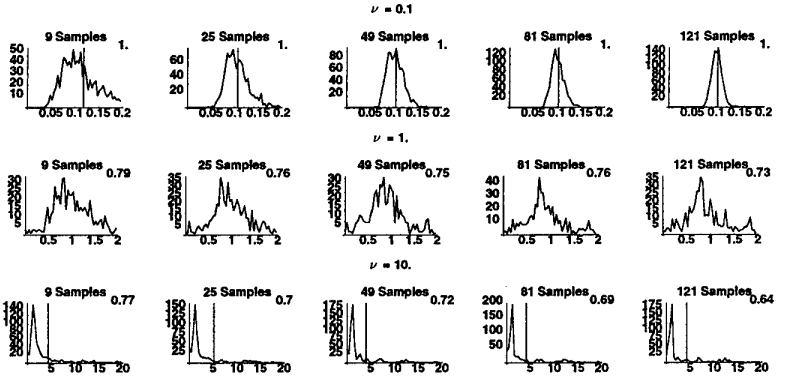

(b) $L = 2$

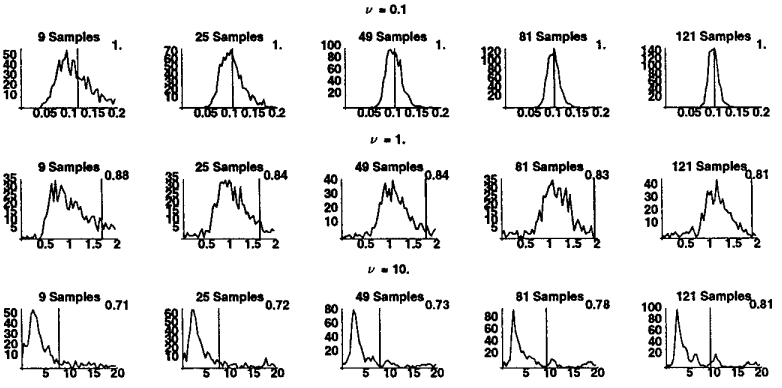

(c) $L = 4$

Figure 11: Plots of the histogram of estimated order using the approximate maximum likelihood estimator (30) for the cases of $\nu = 0.1$, $\nu = 1.0$ and $\nu = 10.0$ for 9, 25, 49, 81 and 121 sample sizes and $L = 1, 2, 4$ calculated over 1000 simulations with $\mu = 1$. The 5%-trimmed mean of each of the 1000 order estimates occurs at the value designated by a vertical line. The number in the upper right-hand corner of each histogram indicates the proportion of the 1000 simulations that gave a reasonable order estimate ($0 < \nu < 10^5$) indicating a varying radar cross-section under the K distribution model.

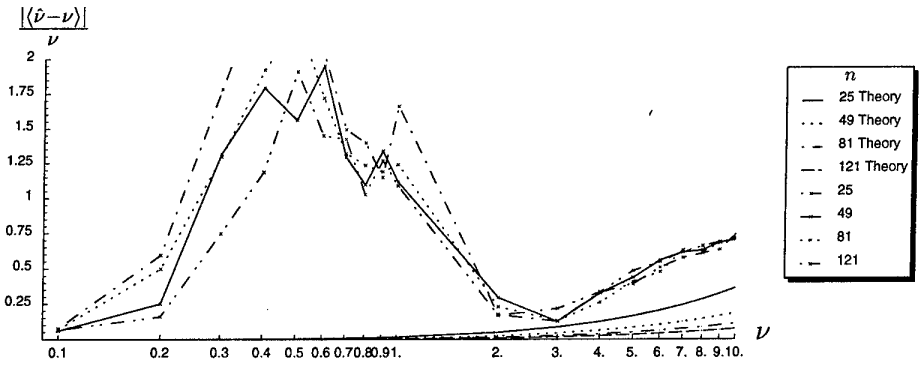

(a) $L = 1$

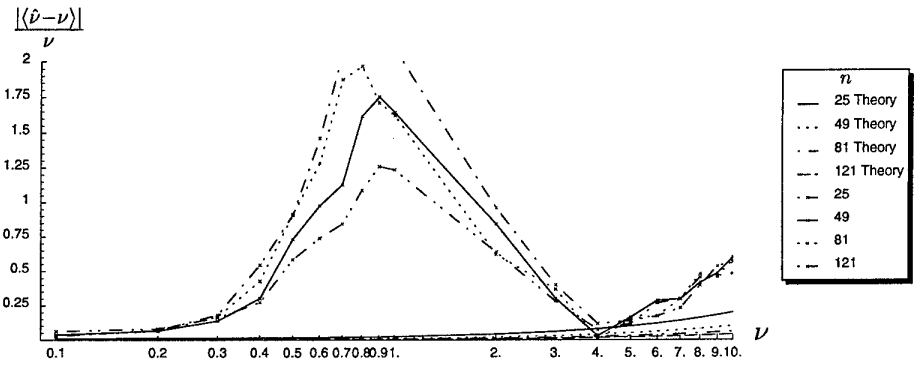

(b) $L = 2$

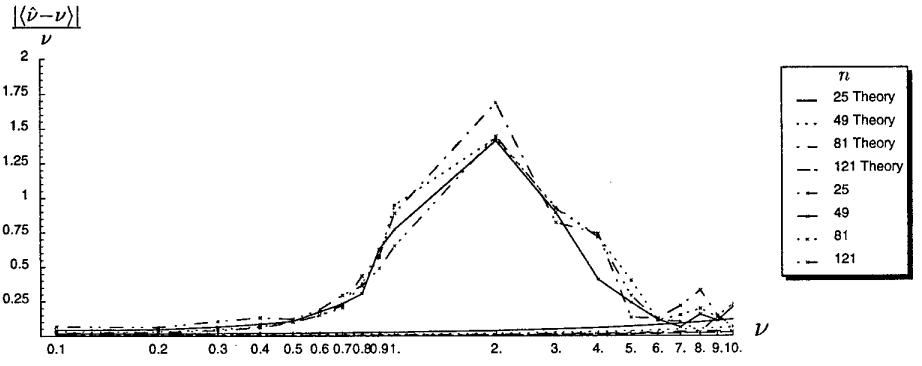

(c) $L = 4$

Figure 12: The absolute value of the relative bias of the estimated order using the approximate maximum likelihood estimator (30) as it varies with ν computed over 1000 simulations with $\mu = 1$. This is plotted against the predicted absolute value of the relative bias (33).

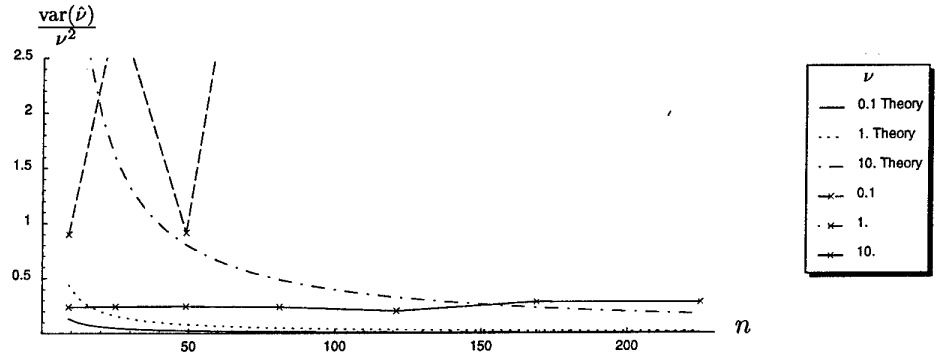

(a) $L = 1$

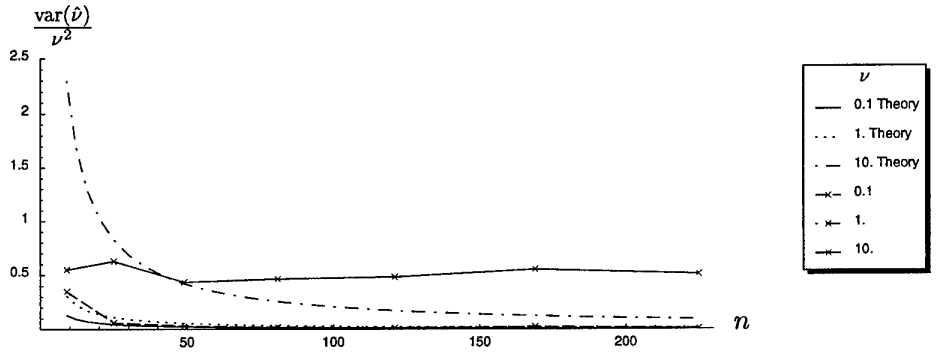

(b) $L = 2$

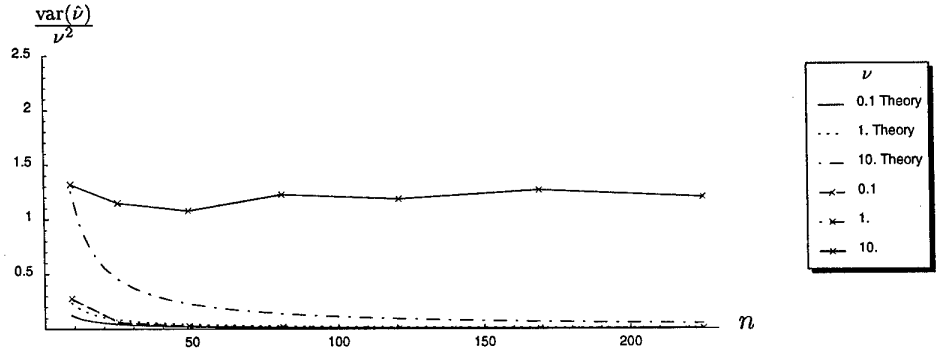

(c) $L = 4$

Figure 13: The normalized variance of the estimated order using the approximate maximum likelihood estimators (30) as it varies with sample size computed over 1000 simulations with $\mu = 1$ and $L = 1, 2, 4$. The theoretical (32) and measured values of the normalized variance of the order estimates are shown for three different values of the order parameter.

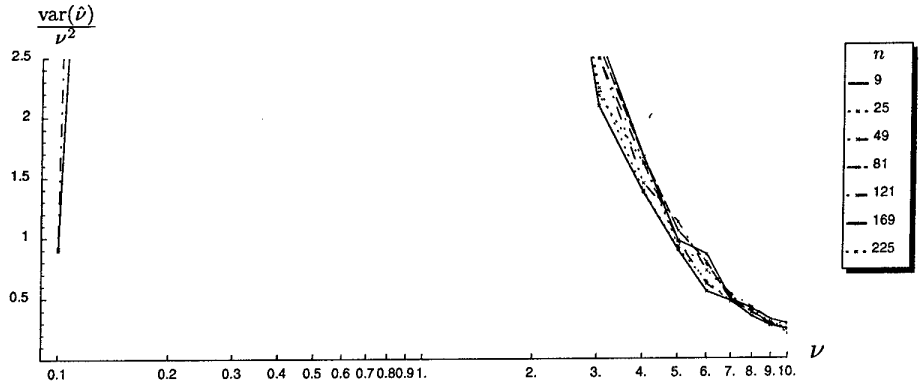

(a) $L = 1$

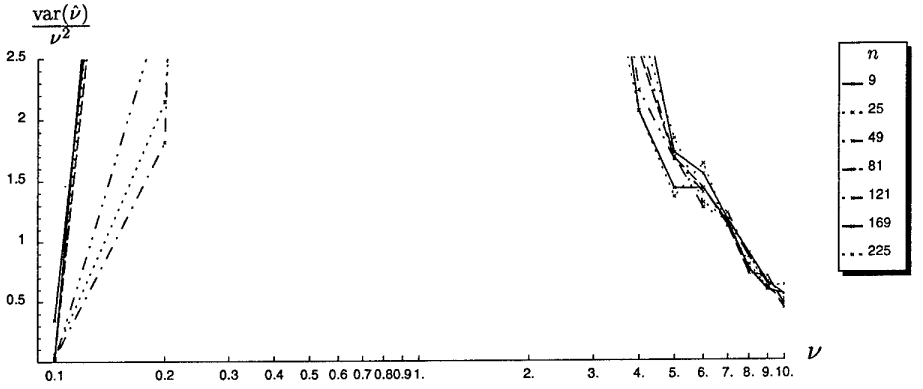

(b) $L = 2$

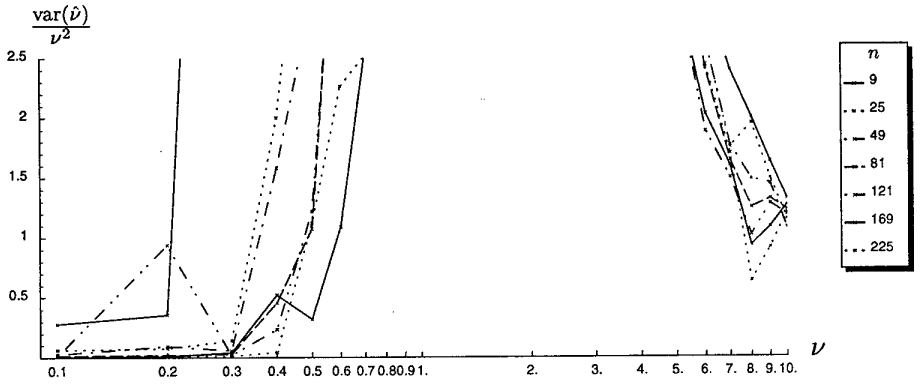

(c) $L = 4$

Figure 14: The normalized variance of the estimated order using the approximate maximum likelihood estimators (30) as it varies with ν computed over 1000 simulations with $\mu = 1$ and $L = 1, 2, 4$.

5.4 Raghavan's Method

Raghavan [32] estimates the parameters of the K distribution by determining the maximum likelihood estimates of a gamma distribution and transforming these estimates into the closest matching K distribution parameters. The maximum likelihood parameters of a gamma distribution can be computed from simply the sample and geometric mean of the data. His approach is as follows (see also [17]).

Firstly, Raghavan shows that it is possible to compute the maximum likelihood estimates for the parameters of a gamma distribution directly from the ratio of the sample (or arithmetic) mean to the geometric mean of the data, defined by

$$\varrho_n = \frac{\frac{1}{n}\sum_{i=1}^{n} x_i}{\left(\prod_{i=1}^{n} x_i\right)^{\frac{1}{n}}}. \tag{35}$$

His argument is then that if the gamma distribution is very similar to the K distribution (for at least some of its parameter values), then the expected value of ϱ_n for the K distribution should give reasonable estimates of its parameters. The expected value of ϱ_n for the K distribution (assuming samples x_i are independent) is given by

$$\begin{aligned}\langle \varrho_n \rangle &= \frac{1}{n}\left\langle \frac{\sum_{i=1}^{n} x_i}{\left(\prod_{i=1}^{n} x_i\right)^{\frac{1}{n}}} \right\rangle = \frac{1}{n}\left\langle \sum_{i=1}^{n} \frac{1}{x_i^{\frac{1}{n}-1} \prod\limits_{\substack{j=1 \\ j\neq i}}^{n} x_j^{\frac{1}{n}}} \right\rangle = \left\langle x_i^{1-\frac{1}{n}} \right\rangle \left\langle x_j^{-\frac{1}{n}} \right\rangle^{n-1} \\ &= \frac{\Gamma(L-\frac{1}{n}+1)\Gamma(\nu-\frac{1}{n}+1)}{\Gamma(L-\frac{1}{n})\Gamma(\nu-\frac{1}{n})} \left(\frac{\Gamma(L-\frac{1}{n})\Gamma(\nu-\frac{1}{n})}{\Gamma(L)\Gamma(\nu)} \right)^{n} \qquad \text{if } \nu > \frac{1}{n} \end{aligned} \tag{36}$$

which differs from the expression in [32] because Raghavan uses the probability density function for a single look amplitude random variable rather than the multi-look intensity random variable used throughout this report. So by computing ϱ_n from (35), an estimate of ν for the K distribution can be found by solving (36) numerically. A plot of $\langle \varrho_n \rangle$ for a range of ν is shown is figure 15. The high slope of this figure for small values of ν indicates that accurate estimates of ν are possible if the variability of ϱ_n is small. Conversely, for larger ν, the slope is very small, so accurate estimates will be difficult (if not impossible) to obtain.

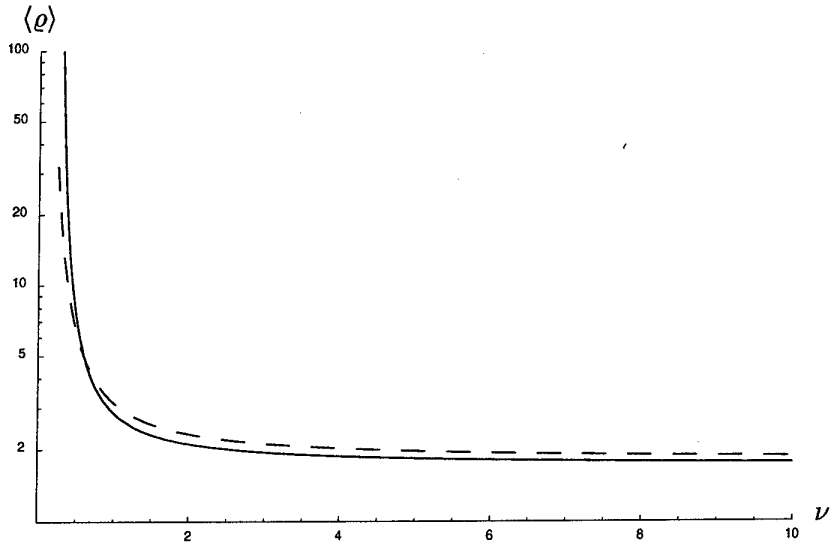

Figure 15: A plot of $\langle\varrho\rangle$ versus ν for $n = 4$ (smooth curve) and $n = 100$ (dashed curve) in the single look case ($L = 1$).

This variability can be examined using the second moment of ϱ_n which is given by

$$\begin{aligned}
\langle\varrho_n^2\rangle &= \frac{1}{n^2}\left\langle \frac{\left(\sum_{i=1}^{n} x_i\right)^2}{\prod_{i=1}^{n} x_i^{\frac{2}{n}}} \right\rangle = \frac{1}{n^2}\left\langle \frac{\sum_{i=1}^{n} x_i^2 + \sum_{i=1}^{n}\sum_{\substack{j=1 \\ j\neq i}}^{n} x_i x_j}{\prod_{i=1}^{n} x_i^{\frac{2}{n}}} \right\rangle \\
&= \frac{1}{n^2}\left\langle \sum_{i=1}^{n} \frac{1}{x_i^{\frac{2}{n}-2} \prod_{\substack{j=1 \\ j\neq i}}^{n} x_j^{\frac{2}{n}}} + \sum_{i=1}^{n}\sum_{\substack{j=1 \\ j\neq i}}^{n} \frac{1}{x_i^{\frac{2}{n}-1} x_j^{\frac{2}{n}-1} \prod_{\substack{k=1 \\ k\neq i \\ k\neq j}}^{n} x_k^{\frac{2}{n}}} \right\rangle \\
&= \frac{1}{n^2}\left(n\left\langle \frac{1}{x_i^{\frac{2}{n}-2}} \right\rangle \left\langle \frac{1}{x_j^{\frac{2}{n}}} \right\rangle^{n-1} + n(n-1)\left\langle \frac{1}{x_i^{\frac{2}{n}-1}} \right\rangle^2 \left\langle \frac{1}{x_k^{\frac{2}{n}}} \right\rangle^{n-2} \right) \\
&= \frac{\left(\Gamma(L-\frac{2}{n})\Gamma(\nu-\frac{2}{n})\right)^{n-2}}{n\left(\Gamma(L)\Gamma(\nu)\right)^n} \left((n-1)\left(\Gamma(L-\frac{2}{n}+1)\Gamma(\nu-\frac{2}{n}+1)\right)^2 + \right. \\
&\qquad \left. \Gamma(L-\frac{2}{n})\Gamma(L-\frac{2}{n}+2)\Gamma(\nu-\frac{2}{n})\Gamma(\nu-\frac{2}{n}+2) \right)
\end{aligned} \tag{37}$$

which again differs from [32] for the reasons expressed above. Plotting $\langle\varrho_n^2\rangle/\langle\varrho_n\rangle^2$ versus ν for different values of n shown in figure 16 indicates that for a sample size of 25, the variance of ϱ_n is less than 5 percent of the square of its mean approximately for all $\nu > 1.5$. Unfortunately, this also corresponds to the region of small slope and so inaccurate inversion of ϱ to estimate ν will result.

In section 5.7 we will consider a mathematically equivalent estimator in the log domain,

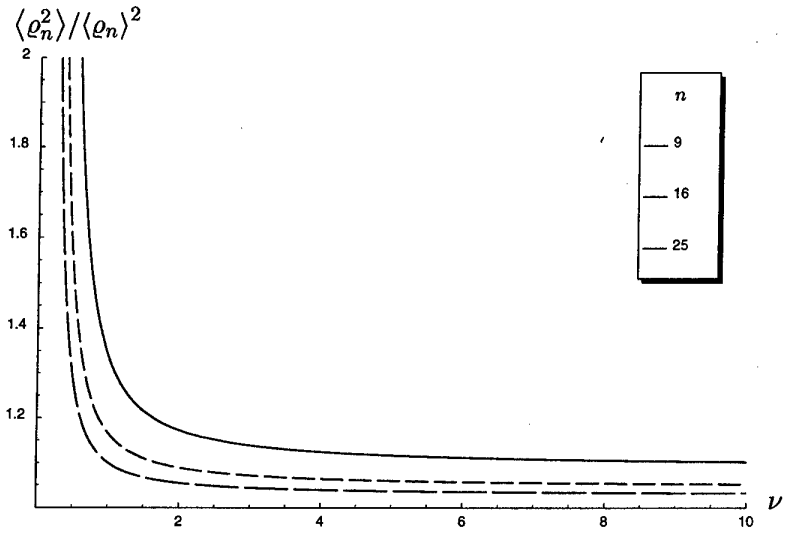

Figure 16: A plot of $\langle \varrho_n^2 \rangle / \langle \varrho_n \rangle^2$ versus ν for different sample sizes in the single look case ($L = 1$).

which is the approach that seems to have gained greater acceptance. As a consequence, we will not examine the performance of an estimator for ν based on (36) here through simulation. However, the above analysis serves to foreshadow the problems that plague other estimators of the order parameter. They are firstly, the variance of a measure (in this case ϱ) with ν, and secondly, the highly nonlinear process of inverting the measure to determine the estimate $\hat{\nu}$. We will consider the latter problem in more detail in section 5.9.2.

5.5 Second and Fourth Moments

Another approach to estimating ν uses the second and fourth moments [17]. The ratio of the fourth moment to the square of the second moment from (6) is given by

$$\frac{\langle x^4 \rangle}{\langle x^2 \rangle^2} = \frac{(L+2)(L+3)(\nu+2)(\nu+3)}{L(L+1)\nu(\nu+1)} \tag{38}$$

which can be solved analytically for $\hat{\nu}$, the estimate of ν, using sample estimates $\langle x_i^2 \rangle$ and $\langle x_i^4 \rangle$ for the two moments. The parameter μ would be estimated by $\langle x_i \rangle$, the sample mean. (The form of this is different in [17] again due to the moments used there being for the K distributed amplitude random variable rather than the intensity random variable that is used here). This estimator's dependence upon the fourth moment makes it unsuitable for small sample sizes because of higher moment's higher variability. Raghavan [32] points out that any ratio of moments of order $2m$ and m could achieve a similar estimator for ν but of course the variability of the estimates worsen with increasing m. As a consequence, (38) seems to have nothing to offer over a method based on the first and second moment, which we consider next.

5.6 First and Second Moments

The next approach we consider here uses the ratio of the second central moment to the square of the first moment [17,27] which for the K distribution is given by

$$\frac{\langle x^2 \rangle - \langle x \rangle^2}{\langle x \rangle^2} = (1 + \frac{1}{L})(1 + \frac{1}{\nu}) - 1. \tag{39}$$

So if we define the measure V to be[2]

$$V \triangleq \frac{\langle x_i^2 \rangle - \langle x_i \rangle^2}{\langle x_i \rangle^2} \tag{40}$$

from the sample moments, then an estimate $\hat{\nu}$ can be determined from

$$V = (1 + \frac{1}{L})(1 + \frac{1}{\hat{\nu}}) - 1. \tag{41}$$

This estimator was termed the *contrast* by Oliver because it is the ratio of the variance of the sample to the square of its mean. We would expect there to be less variability in this estimate than the one from (38) because of the smaller variance of sample estimates of first and second moments as compared with second and fourth moments. (Note that in [17] the ratio of these moments for the K distributed amplitude random variable requires a numerical search to determine $\hat{\nu}$.)

The approximate bias and error in the order parameter is given by [27]

$$\langle \hat{\nu} - \nu \rangle \approx -\frac{\nu^2}{n}\left(1 + \frac{1}{\nu}\right)\left(\frac{1}{\nu} + \frac{1}{L} + \frac{5}{L\nu}\right) \tag{42}$$

and [3]

$$\frac{\mathrm{var}(\hat{\nu})}{\nu^2} \approx \frac{2\nu^2 L}{n(1+L)}\left(1 + \frac{1}{\nu}\right)\left(\frac{1}{\nu} + \frac{1}{L} + \frac{3}{L\nu}\right)\left(\frac{1}{\nu} + \frac{1}{L} + \frac{4}{L\nu}\right) \tag{43}$$

respectively to first order in $1/n$.

Figure 17 plots the histogram of estimated order values using (41) from 1000 simulations for various values of the order ν and differing sample sizes for $L = 1, 2, 4$. For small sample sizes (25 and less), and large order ($\nu = 10.0$), figure 17 shows that roughly 30–70% of the estimates of ν (one minus the number in the upper right hand corner of each histogram) are deemed to be due to a constant radar cross-section (*i.e.* $\nu = \infty$). (The test conditions to determine this were the same as for the approximate maximum likelihood estimator (30): a negative value of ν, or one larger than 10^5.) This improves with multi-looking, so that for four looks, and sample sizes of 49 and larger, the proportion of constant radar cross section estimates drops to below 10%. A trimmed mean was used for the same reason as discussed for figure 11 in section 5.3.

Figure 18 plots the absolute value of the relative bias of the order estimate against the actual order parameter. There is a clear bias in the order estimate from V, and this bias is

[2]The measure V expressed in terms of the moments of the K distribution as in (39) is not a random variable but we can only estimate it from sample moments, so strictly speaking the measure in (40) and (41) is an estimate, so by convention V in these equations should be denoted by $\hat{V}$.

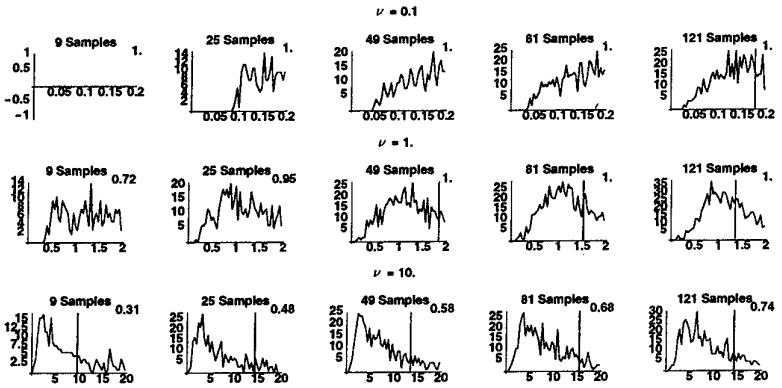

(a) $L = 1$

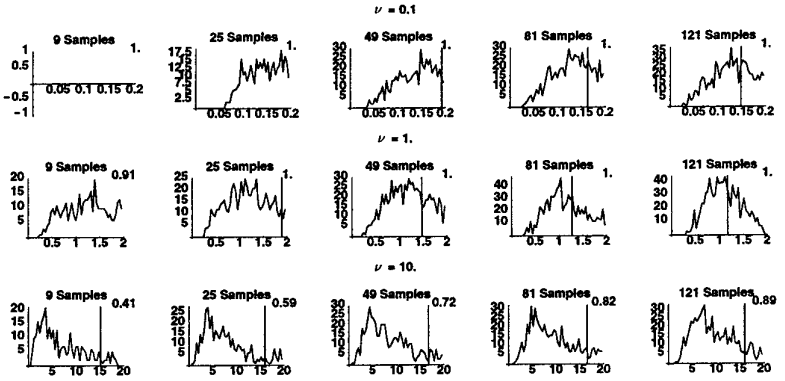

(b) $L = 2$

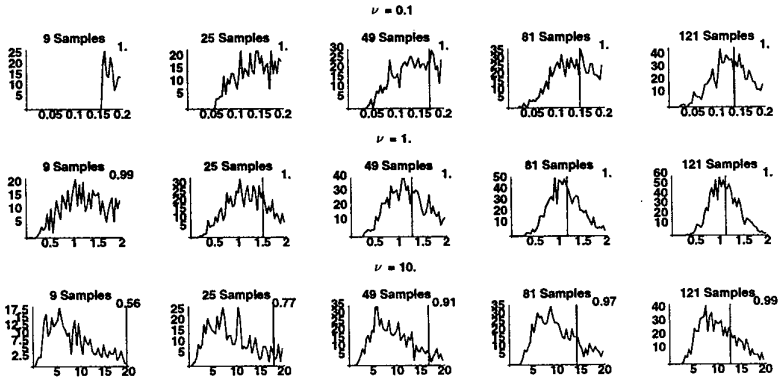

(c) $L = 4$

Figure 17: Plots of the histogram of estimated order using measure V (41) for the cases of $\nu = 0.1$, $\nu = 1.0$ and $\nu = 10.0$ for 9, 25, 49, 81 and 121 sample sizes and $L = 1, 2, 4$ calculated over 1000 simulations with $\mu = 1$. The 5%-trimmed mean of each of the 1000 order estimates occurs at the value designated by a vertical line. The number in the upper right-hand corner of each histogram indicates the proportion of the 1000 simulations that gave a reasonable order estimate $(0 < \nu < 10^5)$ indicating a varying radar cross-section under the K distribution model.

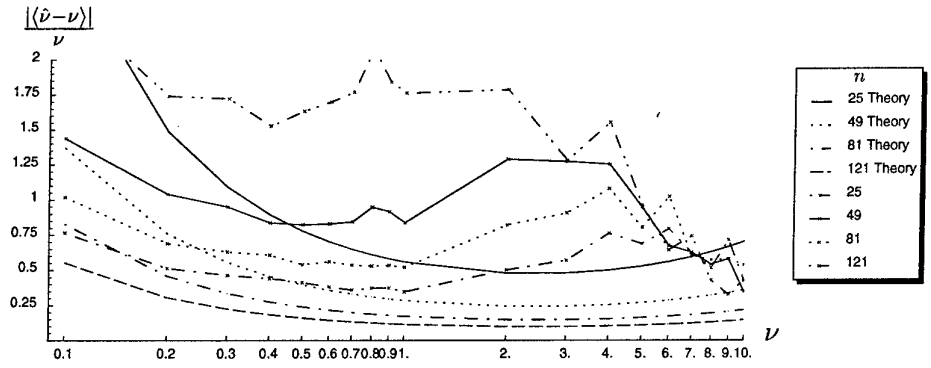

(a) $L = 1$

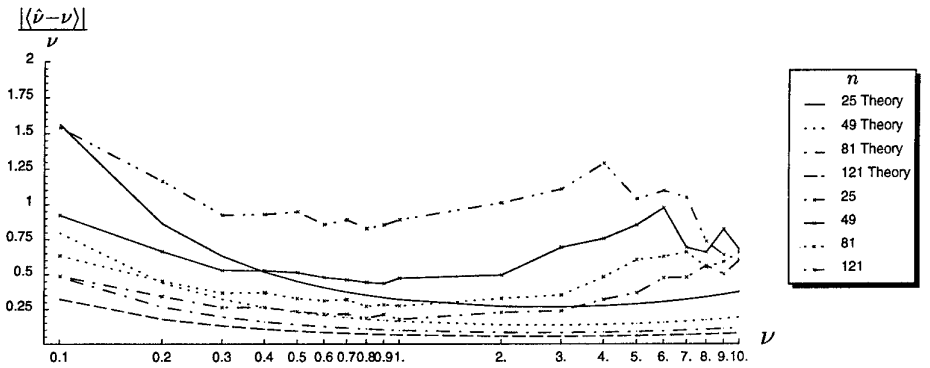

(b) $L = 2$

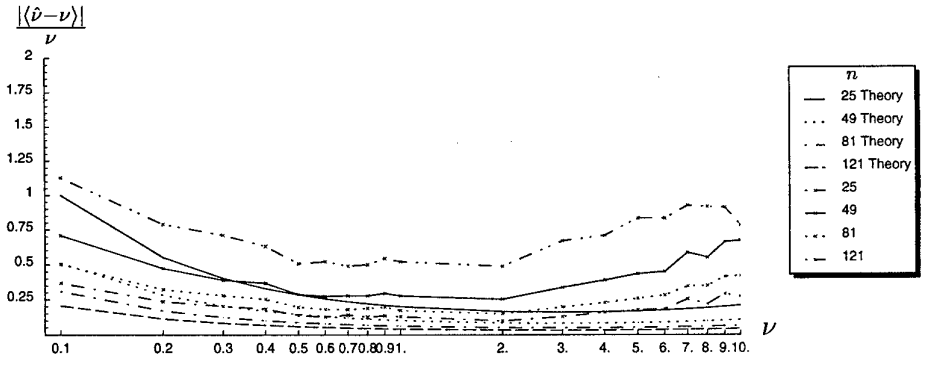

(c) $L = 4$

Figure 18: The absolute value of the relative bias of the estimated order using measure V (41) as it varies with ν computed over 1000 simulations with $\mu = 1$ with sample sizes of $25, 49, 81, 121$, and $L = 1, 2, 4$. These are plotted against the predicted absolute value of the relative bias (42).

only in agreement with that predicted by (42) for very small values of the order parameter ($\nu \approx 0.1$), at least over the small sample sizes up to 121 pixels. Relative bias decreases with increasing number of looks, and shows a complicated bi-modal trend with increasing order in the single look case that is not accounted for by theory (42). However, the trend with ν in the multi-look cases is more consistent with theory, although still larger than that predicted.

Figure 19 plots the normalized variance of the order parameter estimate computed during each of the 1000 simulations against the theoretical normalized variance of the order from (43). The only time the predicted normalized variance (42) matches that measured is for $\nu = 1.0$. In the case of $\nu = 10.0$, the normalized variance is much larger (off the scale for all but the highest sample sizes in the four-look case), and smaller than that predicted in the case of $\nu = 0.1$. Multi-looking improves the normalized variance of the estimate $\hat{\nu}$, which can be seen also in figure 20, with the normalized variance of the order estimate against the order parameter.

5.7 Normalized Logarithm of Intensity

The approximate maximum likelihood estimator for the order parameter in (30) is dominated by the expected value of the log of the data. Consequently, Oliver [27] has suggested an estimator for the order parameter ν in these terms. The mean value of the logarithm of the intensity x is given by

$$\langle \log x \rangle = \log \langle x \rangle - \log \nu + \psi^{(0)}(\nu) + \psi^{(0)}(L) - \log L \tag{44}$$

from the probability density function of the K distribution. In situations where there is no prior knowledge of the parameters or moments, we estimate $\langle \log x \rangle$ and $\langle x \rangle$ from the sample data. Rearranging, using sample moments we obtain

$$\log \langle x_i \rangle - \langle \log x_i \rangle = \log \hat{\nu} - \psi^{(0)}(\hat{\nu}) + \log L - \psi^{(0)}(L) \tag{45}$$

which can be solved for $\hat{\nu}$, the estimate of ν. The texture measure U, termed the *normalized logarithm of intensity*, is therefore defined to be

$$U \triangleq \log \langle x_i \rangle - \langle \log x_i \rangle. \tag{46}$$

So then

$$U = \log \hat{\nu} - \psi^{(0)}(\hat{\nu}) + \log L - \psi^{(0)}(L). \tag{47}$$

Raghavan's method is mathematically equivalent to this approach because taking the log of the geometric mean is the same as computing the sample mean of log of the data.

The approximate bias and variance in the order parameter to first order in $1/n$ by this estimate is

$$\langle \hat{\nu} - \nu \rangle \approx \frac{1 + (1+\nu)/L}{2n(1 - \nu\psi^{(1)}(\nu))} \tag{48}$$

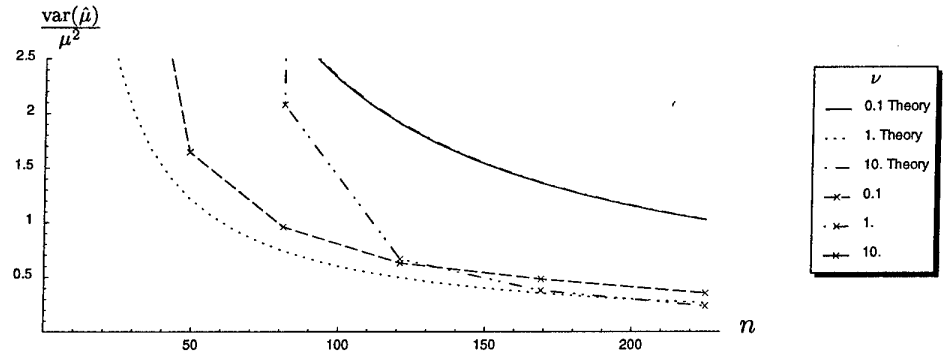

(a) $L = 1$

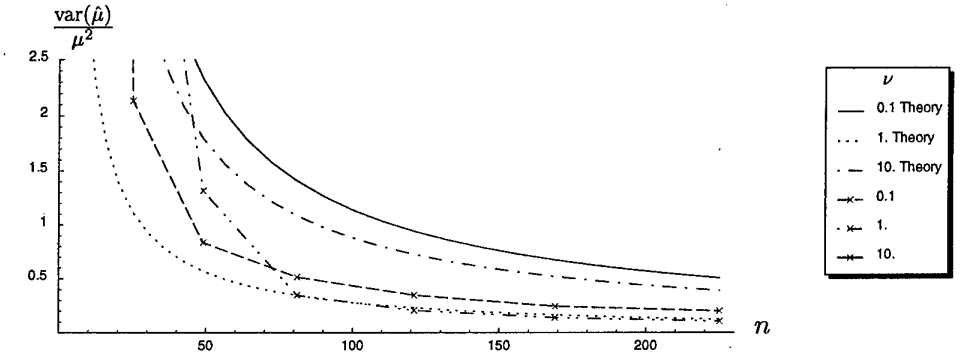

(b) $L = 2$

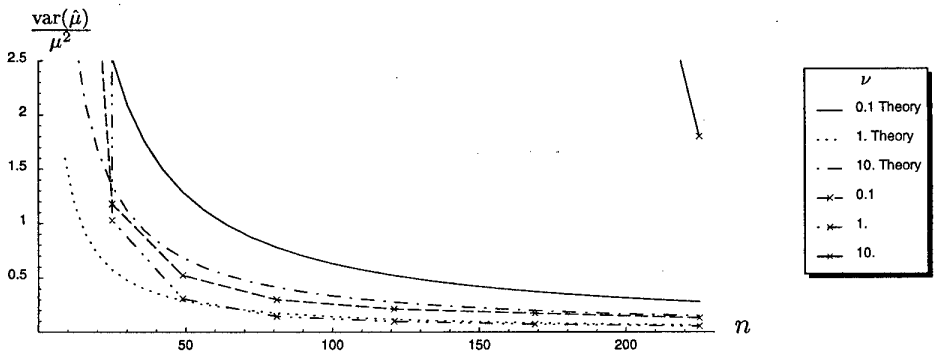

(c) $L = 4$

Figure 19: The normalized variance of the estimated order using measure V (41) as it varies with sample size and $L = 1, 2, 4$ each computed over 1000 simulations with $\mu = 1$. The theoretical (43) and calculated values of the normalized variance of the order estimates are shown for the three different values of the order parameter in each plot.

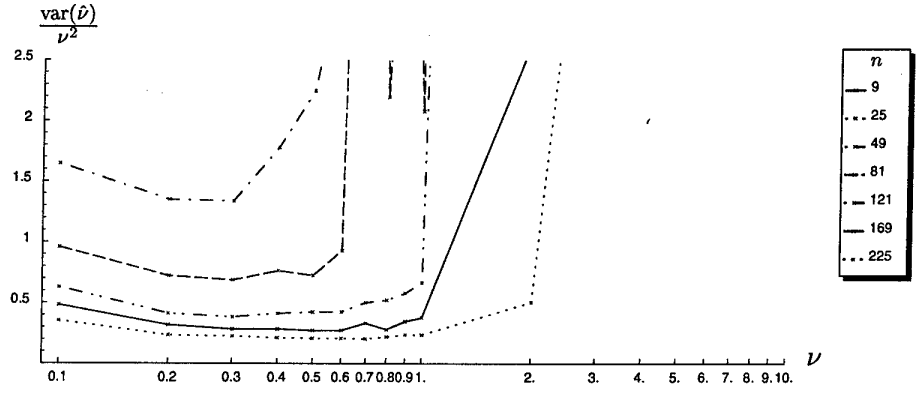

(a) $L = 1$

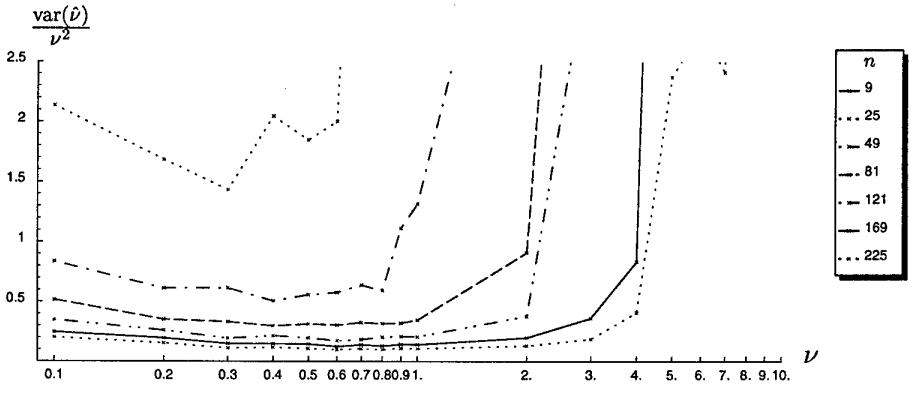

(b) $L = 2$

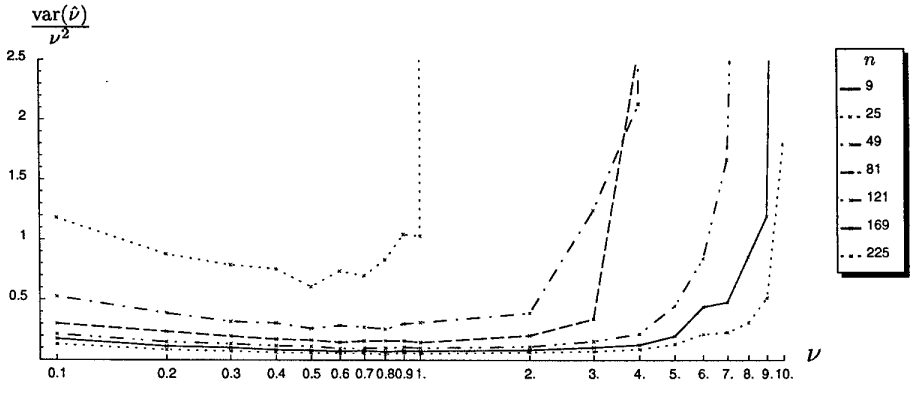

(c) $L = 4$

Figure 20: The normalized variance of the estimated order using measure V (41) as it varies with ν computed over 1000 simulations with $\mu = 1$, varying sample sizes and $L = 1, 2, 4$.

and

$$\frac{\mathrm{var}(\hat{\nu})}{\nu^2} \approx \frac{\nu\psi^{(1)}(\nu) - 1 + \nu\psi^{(1)}(L) + (1-\nu)/L}{n\nu(1-\nu\psi^{(1)}(\nu))^2} \tag{49}$$

respectively.

Figure 21 plots the histogram of estimated order values using (47) from 1000 simulations using various values of the order ν and differing number of samples from the distribution for $L = 1, 2, 4$. A trimmed mean was used for the same reasons as discussed for figure 11 in section 5.3. When $\nu = 10.0$ in the single look case, 30–60% of the samples were deemed to be due to a constant radar cross-section. This proportion decreased with increasing looks to be less than 10% in the four-look case for sample sizes of 49 and above. The effect at $\nu = 1.0$ only occurred to any significant extent ($> 2\%$) when the sample size was extremely small (9 samples) for $L = 1$. This performance is slightly better than that of the measure V (figure 17).

Figure 22 plots the absolute value of the relative bias of the order estimate against the actual value of the order parameter. A relative bias is only appreciable for larger values of ν in the range, and the peak moves to the right as the number of looks increases. The number of looks has a small reducing effect upon the relative bias. The predicted relative bias (48) is a poor match with the measured value for ν in the upper range, although for larger sample sizes (81 samples and above) in the lower range of ν ($\nu \leqslant 0.6$) it may be a decent match but it is not possible to be sure from the scale of the graph.

Figure 23 plots the normalized variance of the order parameter estimate computed during the 1000 simulations against the theoretical variance of the order from (49). The measured normalized variance matches the predicted normalized variance (49) even for small sample sizes (25 samples) in the case of $\nu = 0.1$, and for larger sample sizes ($\geqslant 81$ samples) for $\nu = 1.0$. The match between predicted and measured normalized variance improves with increases in the number of looks, which also improves the measured normalized variance of ν overall. The normalized variance in the case of $\nu = 10.0$ is off scale for all but the largest sample size in the four-look case.

Figure 24 plots the normalized variance of the order estimate against the actual order parameter value. The improvement in the normalized variance of the order estimate with increasing sample size and number of looks is apparent for $\nu \geqslant 1.0$. When ν is smaller than this, sample size and number of looks has a much smaller effect on the normalized variance.

Rather than using the sample mean as the estimate of the mean of the distribution, we can instead use the average of the logarithm of the sample using (44). This will also be more convenient in situations where the data is presented on a log scale. We obtain the estimate $\hat{\mu}$ by substituting the estimate $\hat{\nu}$ into (44) with $\langle x \rangle$ replaced by $\hat{\mu}$, to give [3]

$$\log \hat{\mu} = \langle \log x \rangle + \log \nu - \psi^{(0)}(\nu) - \psi^{(0)}(L) + \log L. \tag{50}$$

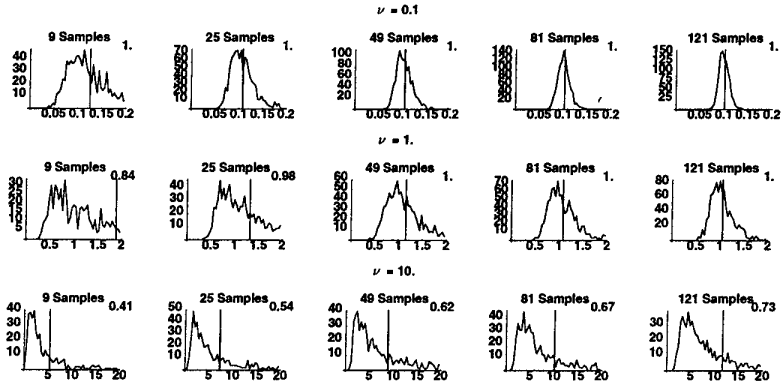

(a) $L = 1$

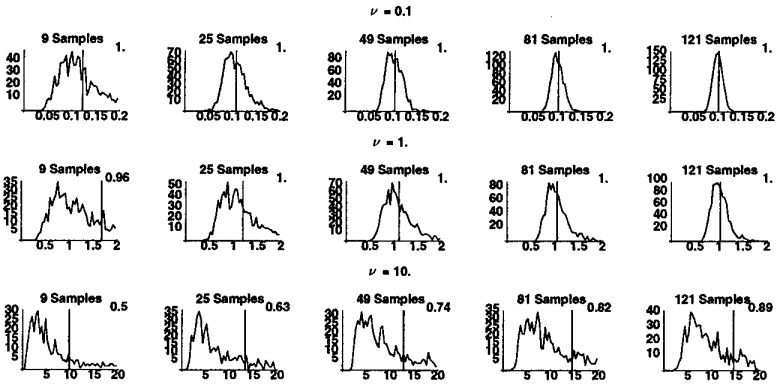

(b) $L = 2$

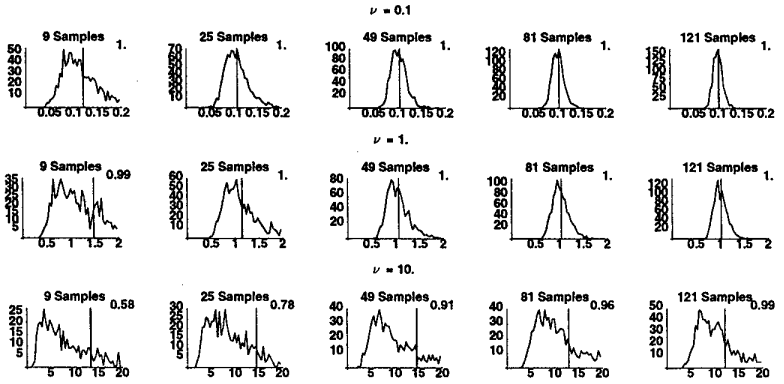

(c) $L = 4$

Figure 21: Plots of the histogram of estimated order using measure U (47) for the cases of $\nu = 0.1$, $\nu = 1.0$ and $\nu = 10.0$ for 9, 25, 49, 81 and 121 sample sizes and $L = 1, 2, 4$ calculated over 1000 simulations with $\mu = 1$. The 5%-trimmed mean of each of the 1000 order estimates ocurs at the value designated by a vertical line. The number in the upper right-hand corner of each histogram indicates the proportion of the 1000 simulations that gave a reasonable order estimate ($0 < \nu < 10^5$) indicating a varying radar cross-section under the K distribution model.

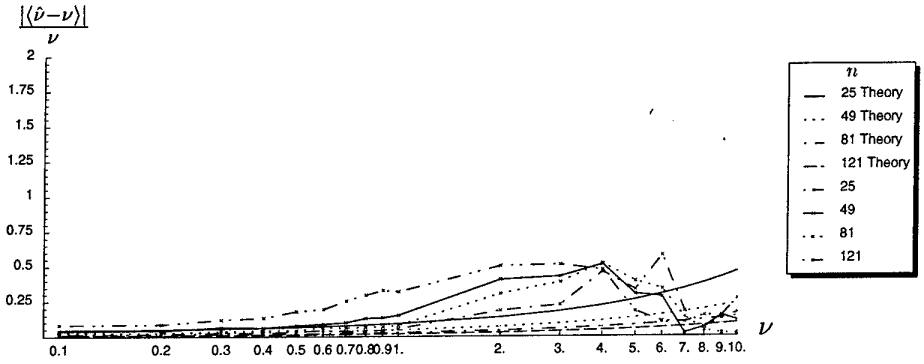

(a) $L = 1$

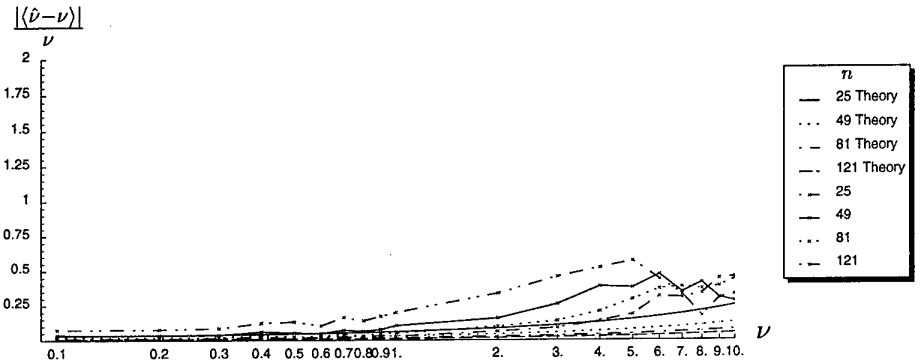

(b) $L = 2$

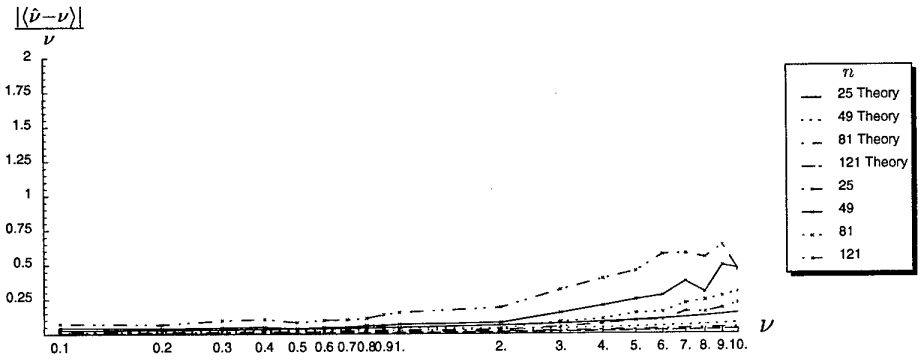

(c) $L = 4$

Figure 22: The absolute value of the relative bias of the estimated order using measure U (47) as it varies with ν computed over 1000 simulations with $\mu = 1$ and sample sizes of 25, 49, 81, and 121, and $L = 1, 2, 4$. These are plotted against the predicted absolute value of the relative bias (48).

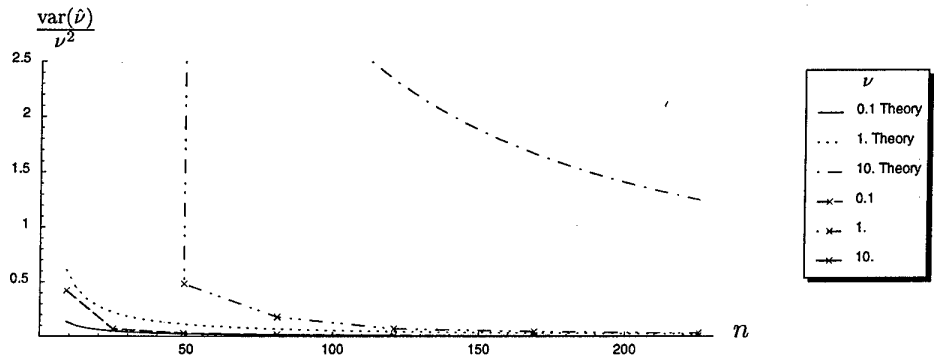

(a) $L = 1$

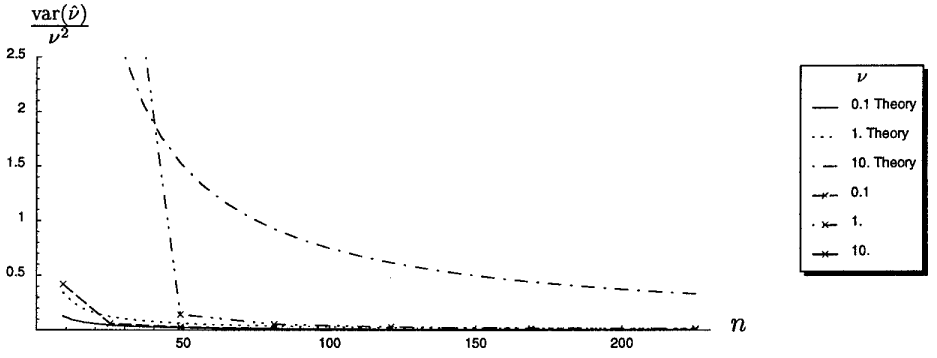

(b) $L = 2$

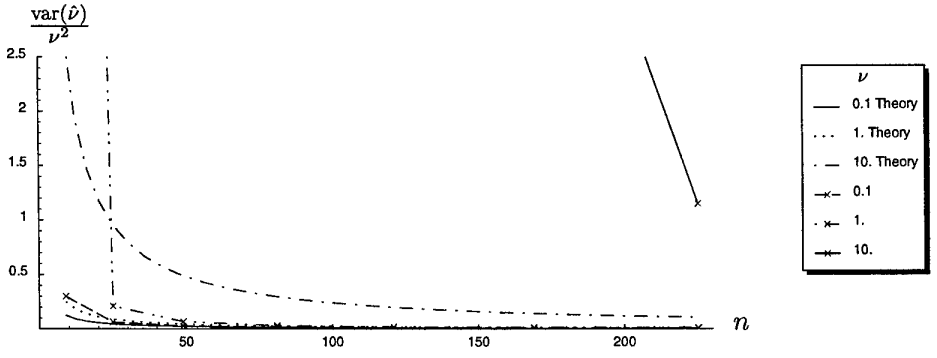

(c) $L = 4$

Figure 23: The normalized variance of the estimated order using measure U (47) as it varies with sample size computed over 1000 simulations with $\mu = 1$. The theoretical (49) and calculated values of the variance of the order estimates are shown for three different values of the order parameter.

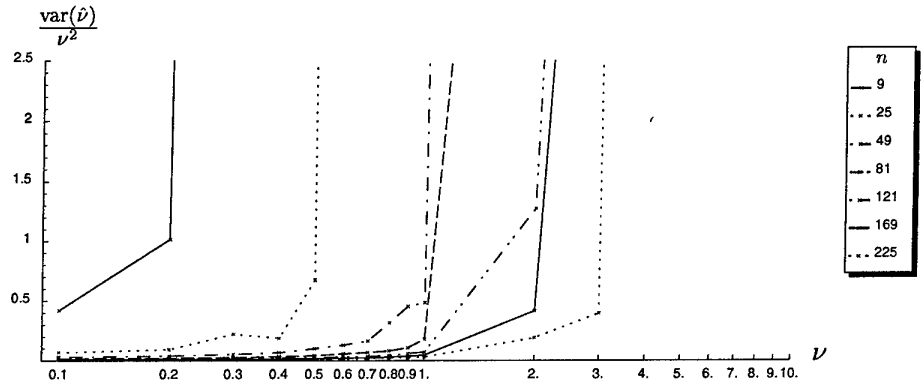

(a) $L = 1$

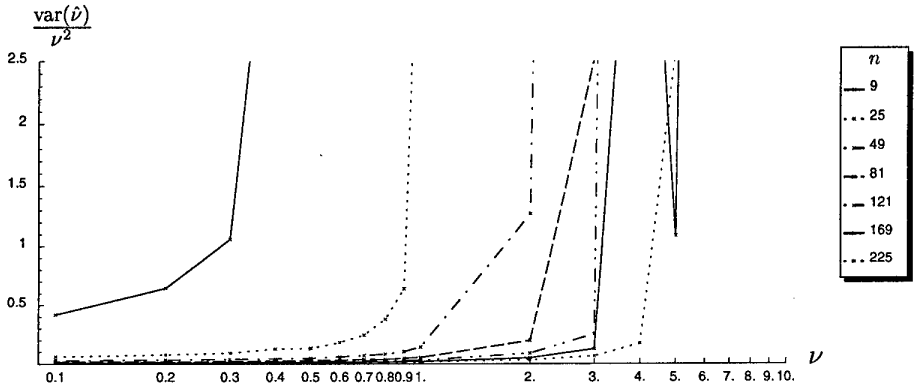

(b) $L = 2$

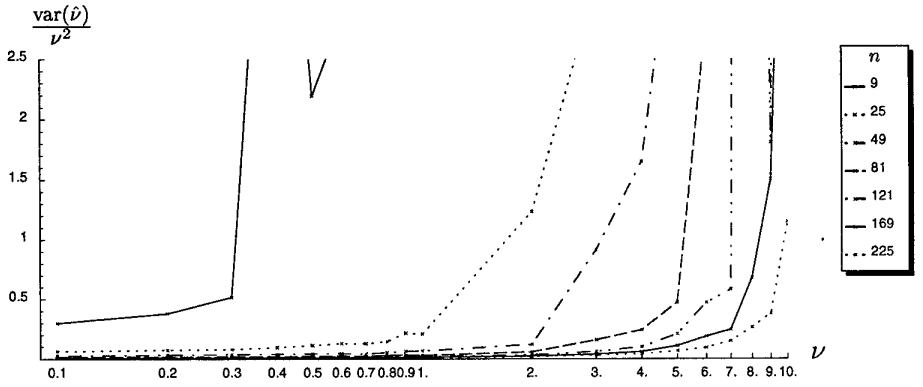

(c) $L = 4$

Figure 24: The normalized variance of the estimated order using measure U (47) as it varies with ν computed over 1000 simulations with $\mu = 1$ for a range of sample sizes and looks $L = 1, 2, 4$.

The normalized variances of this estimate is given by (to first order in $1/n$)

$$\frac{\mathrm{var}(\hat{\mu})}{\mu^2} \approx \frac{1}{n}\left(\psi^{(1)}(\nu)+\psi^{(1)}(L)-2\frac{\nu\psi^{(1)}(\nu)-1}{\nu\psi^{(2)}(\nu)}\left(\psi^{(2)}(\nu)+\psi^{(2)}(L)\right)\right.$$
$$\left.+\left(\frac{\nu\psi^{(1)}(\nu)-1}{\nu\psi^{(2)}(\nu)}\right)^2\left\{\psi^{(3)}(\nu)+\psi^{(3)}(L)+2\left(\psi^{(1)}(\nu)+\psi^{(1)}(L)\right)^2\right\}\right) \quad (51)$$

where $\psi^{(2)}(\cdot)$ and $\psi^{(3)}(\cdot)$ are the tetragamma and pentagamma functions, respectively.

Figure 25 plots the histogram of estimated mean values using (50) from 1000 simulations using various values of the order ν and differing number of samples from the distribution. Simulations were performed using the correct value of ν in (50), so the results presented here are the best possible for this estimator. To get a measure of its performance in most practical circumstances, the simulations should be performed using a value of ν that is also estimated from the data. It seems from observation of figure 25 that there is a bias in the estimate of the mean for small sample sizes and small values of ν across all the looks considered.

Figure 26 plots the normalized variance of the sample mean over the 1000 simulations against its theoretical value (51), indicating a good correspondence, except for small values of ν ($\nu = 0.1$) where the normalized variance is larger than predicted. From these plots and figure 27, which plots the normalized variance of the mean estimate against the actual order parameter, it is clear that increasing the number of looks reduces the normalized variance of the estimates.

5.8 Variance of Logarithm of Intensity

The order parameter of the K distribution can be estimated from the variance of the logarithm of the sample data [3], which is given by

$$\left\langle \log^2 x \right\rangle - \left\langle \log x \right\rangle^2 = \psi^{(1)}(\nu) + \psi^{(1)}(L) \quad (52)$$

from its probability density function using laws of expectation. So if we define the measure W by

$$W \triangleq \left\langle \log^2 x_i \right\rangle - \left\langle \log x_i \right\rangle^2 \quad (53)$$

called the *variance of log* estimator using sample moments of the logarithm of the data, then an estimate $\hat{\nu}$ of the order can be obtained from

$$W = \psi^{(1)}(\hat{\nu}) + \psi^{(1)}(L). \quad (54)$$

The normalized variances of this estimate is given by (to first order in $1/n$)

$$\frac{\mathrm{var}(\hat{\nu})}{\nu^2} \approx \frac{1}{n}\left(\frac{1}{\nu\psi^{(2)}(\nu)}\right)^2\left(\psi^{(3)}(\nu)+\psi^{(3)}(L)+2\left(\psi^{(1)}(\nu)+\psi^{(1)}(L)\right)^2\right). \quad (55)$$

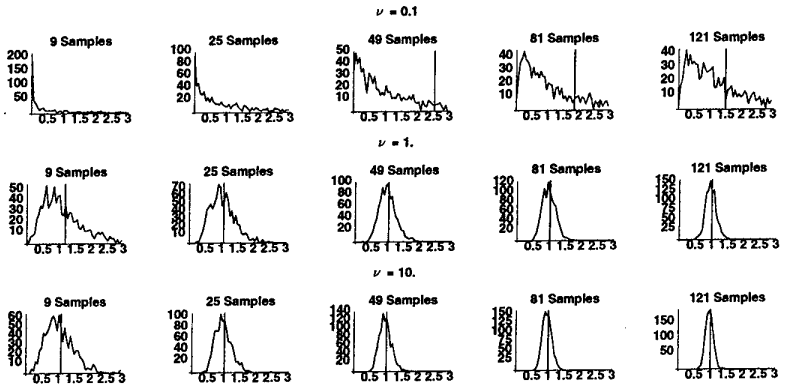

(a) $L = 1$

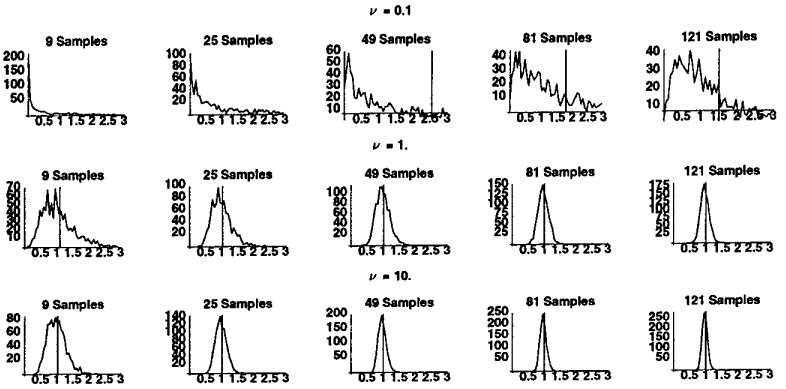

(b) $L = 2$

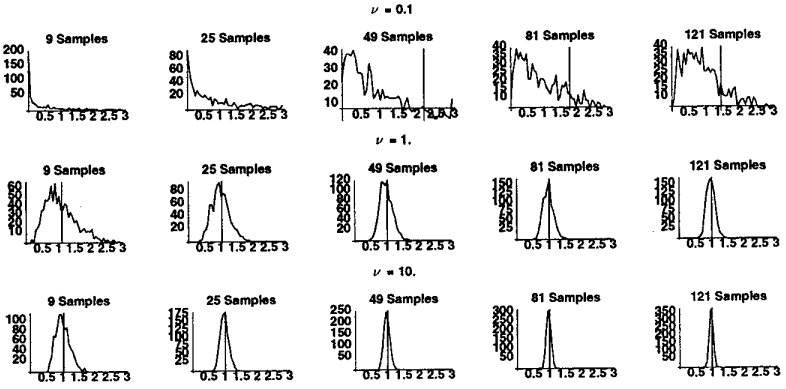

(c) $L = 4$

Figure 25: Plots of the histogram of estimated mean using normalized logarithm of intensity (50) and a priori *knowledge of ν for the cases of $\nu = 0.1$, $\nu = 1.0$ and $\nu = 10.0$ for 9, 25, 49, 81 and 121 sample sizes and $L = 1, 2, 4$, each calculated over 1000 simulations with $\mu = 1$. A vertical line indicates mean estimate of the mean μ obtained over 1000 simulations.*

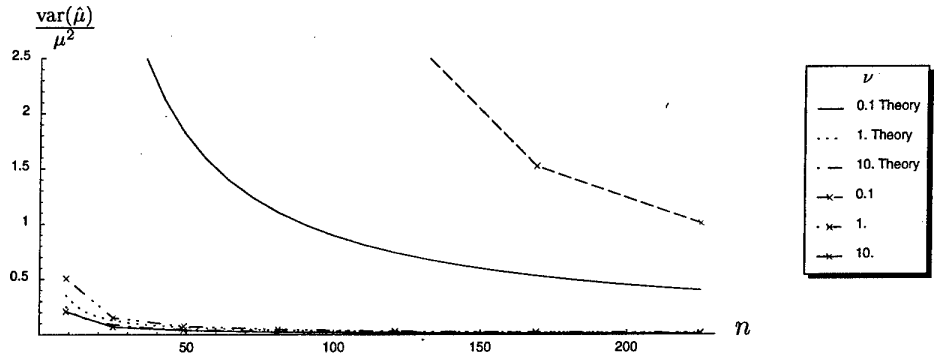

(a) $L = 1$

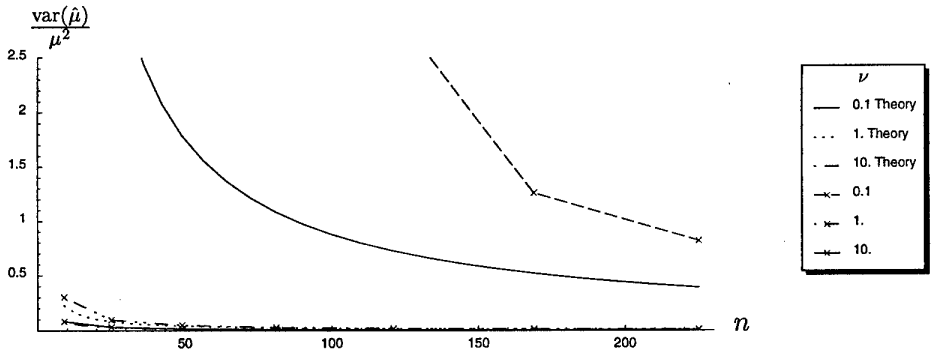

(b) $L = 2$

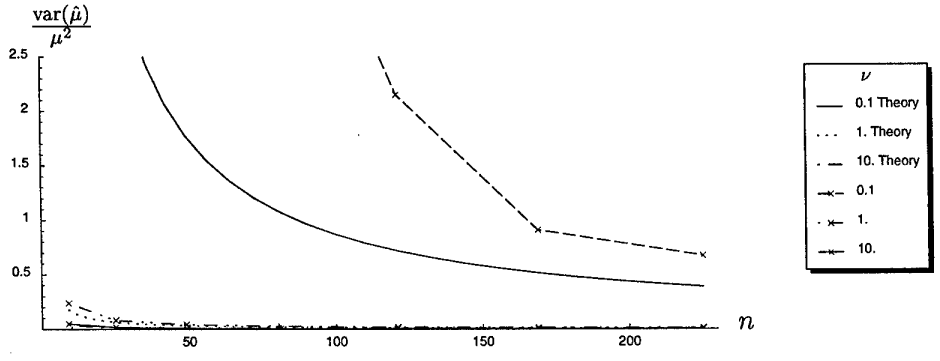

(c) $L = 4$

Figure 26: The normalized variance of the estimated mean using normalized logarithm of intensity (50) as it varies with sample size computed over 1000 simulations, each with $\mu = 1$ for $L = 1, 2, 4$. The theoretical (51) and calculated values of the normalized variance of the mean estimates are shown for three different values of the order parameter.

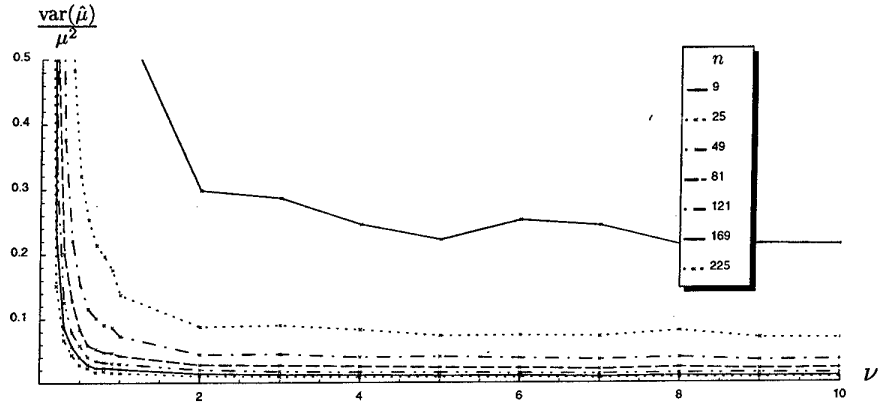

(a) $L = 1$

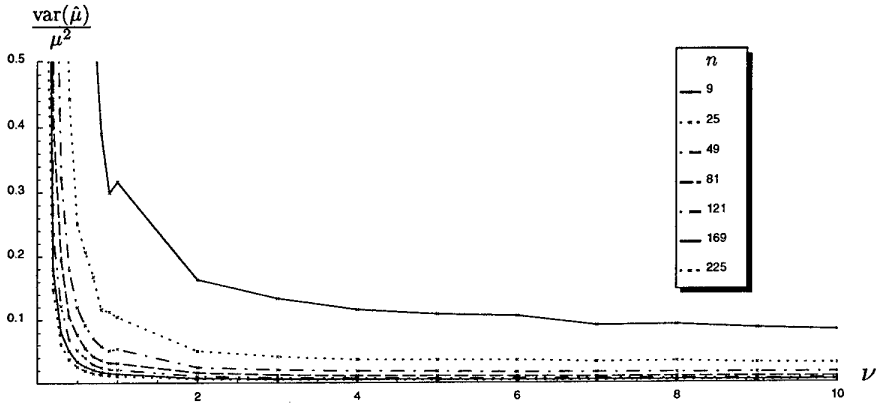

(b) $L = 2$

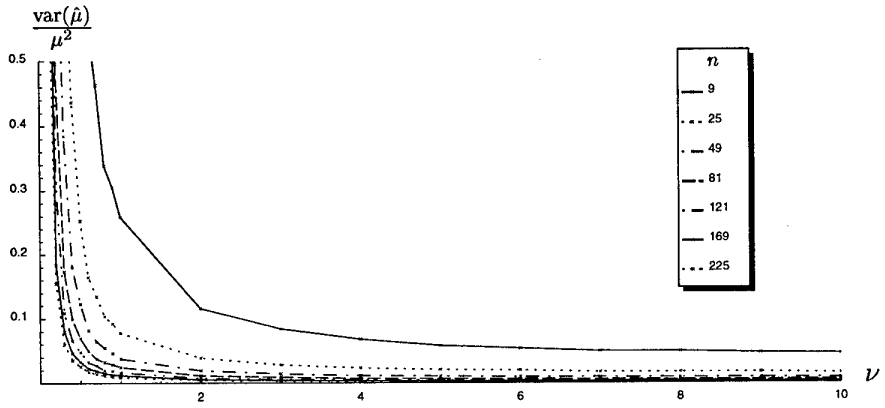

(c) $L = 4$

Figure 27: The normalized variance of the estimated mean using normalized logarithm of intensity (50) as it varies with ν computed over 1000 simulations with $\mu = 1$ for a range of sample sizes and looks $L = 1, 2, 4$.

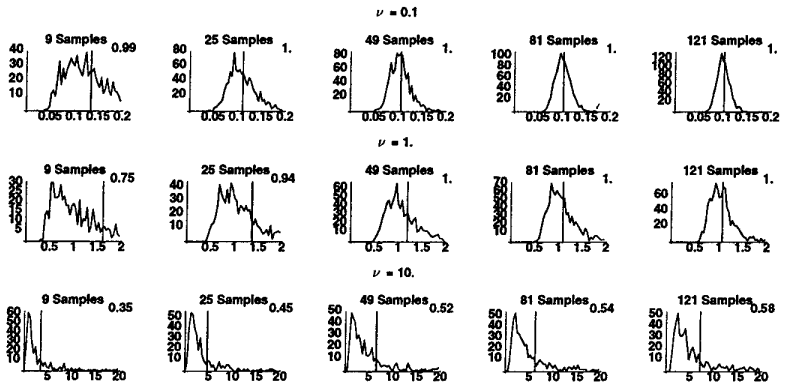

(a) $L = 1$

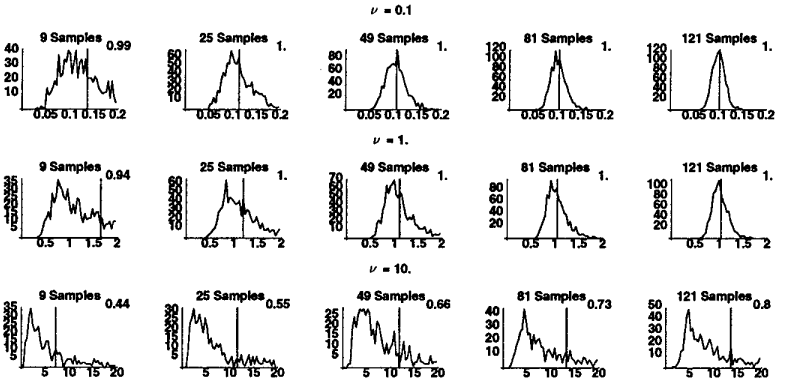

(b) $L = 2$

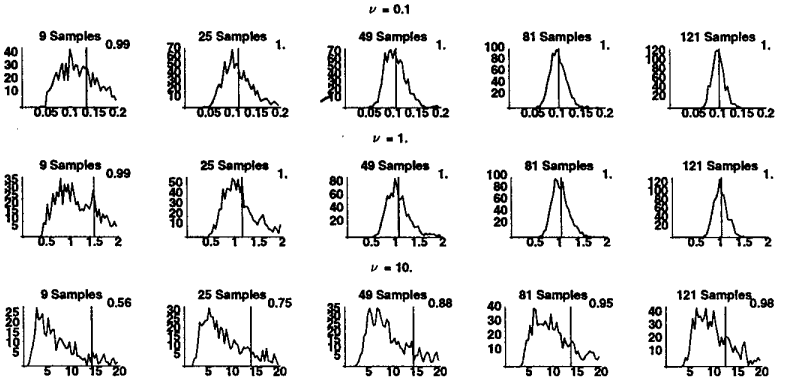

(c) $L = 4$

Figure 28: Plots of the histogram of estimated order using measure W (52) for the cases of $\nu = 0.1$, $\nu = 1.0$ and $\nu = 10.0$ for 9, 25, 49, 81 and 121 sample sizes and $L = 1, 2, 4$ calculated over 1000 simulations with $\mu = 1$. The 5%-trimmed mean of each of the 1000 order estimates occurs at the value designated by a vertical line. The number in the upper right-hand corner of each histogram indicates the proportion of the 1000 simulations that gave a reasonable order estimate ($0 < \nu < 10^5$) indicating a varying radar cross-section under the K distribution model.

Figure 28 plots the histogram of estimated order values using (52) from 1000 simulations using various values of the order ν and differing number of samples from the distribution for $L = 1, 2, 4$. A trimmed mean was used for the same reason as discussed for figure 11 in section 5.3. For $\nu = 10.0$ in the single look case across all sample sizes, in 40–65% of the samples the measure indicated the samples were due to a constant radar cross-section. This proportion decreases for $\nu = 10.0$ as the number of looks increases. For the same sample size, order and number of looks, the proportion of constant radar cross-section determinations is always higher for measure W than for measure U (figure 21), which was itself lower than that of for measure V (figure 17).

Figure 29 plots the absolute value of the relative bias of the order estimate against the actual order parameter value. The relative bias is small for $\nu \leqslant 1.0$ and increases above that value. Increasing the number of looks causes a small improvement in the relative bias in the higher order range ($\nu > 1.0$).

Figure 30 plots the normalized variance of the order parameter estimate computed during the 1000 simulations against the theoretical variance of the order from (55). The measured normalized variance matches the predicted normalized variance (55) for the case of $\nu = 0.1$ even for small sample sizes. As the sample size and number of looks increase, there is a good correspondence in the $\nu = 1.0$ case as well. However, the $\nu = 10.0$ case is much larger than predicted.

Figure 31 plots the normalized variance of the order estimate against the actual order parameter value. For $\nu \geqslant 1.0$, there is a great improvement in the normalized variance of the estimate $\hat{\nu}$ as the number of looks increase. When $\nu < 1.0$, even 25 samples can give reasonable estimates, especially in the multi-look cases ($L = 2, 4$), although measure U (figure 24) looks to be slightly better overall, especially for $\nu > 1.0$.

5.9 Discussion of Estimators

5.9.1 Mean Parameter Estimation

Three methods for estimating the mean have been presented: the sample mean (25), the maximum likelihood estimate for the approximate K distribution (28), and the moment estimate from the normalized logarithm of intensity (50). As discussed by Oliver [27] the sample mean estimate of the K distribution parameter μ is unbiased and has error given by (26). However, the approximate maximum likelihood approach in (28) is biased (with bias given by (33)) and when compared to the variance of the estimator (34) it will become significant when a small number of independent samples are used because the bias is of order $1/n$ from (33) whereas the standard deviation from (34) is of order $1/\sqrt{n}$ [27]. Further, the bias is $\langle \mathbf{x} \rangle / Ln$ and $\langle \mathbf{x} \rangle / 2Ln$ to first order in $1/L$ and $1/n$ in the limit of large ν and small ν, respectively.

The relative bias in the mean estimate from (50) using normalized logarithm of intensity is not given in the literature, but it can be seen empirically from figures 25–27 that it is small when compared with the normalized variance, except perhaps for the smaller sample sizes in the $\nu = 0.1$ cases which are off the scale in figure 25.

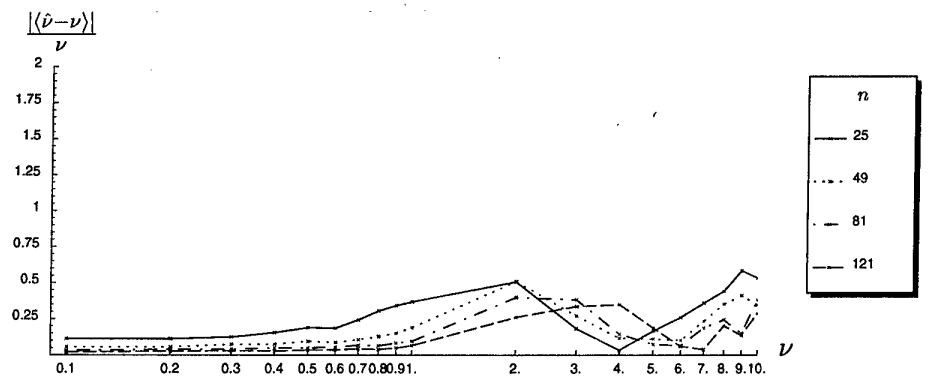

(a) $L = 1$

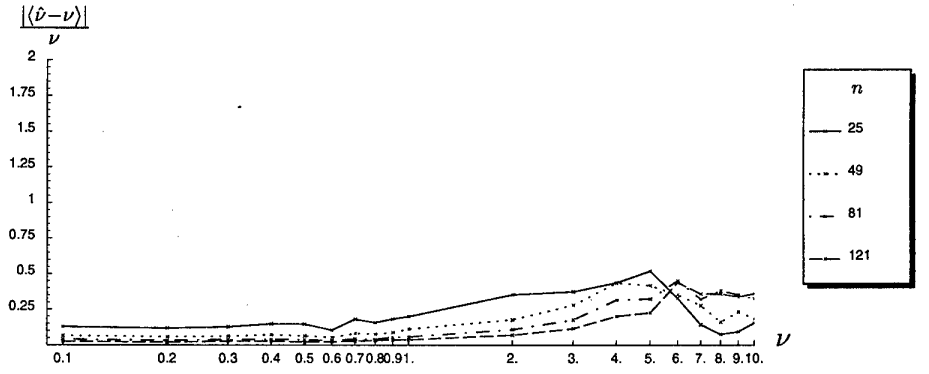

(b) $L = 2$

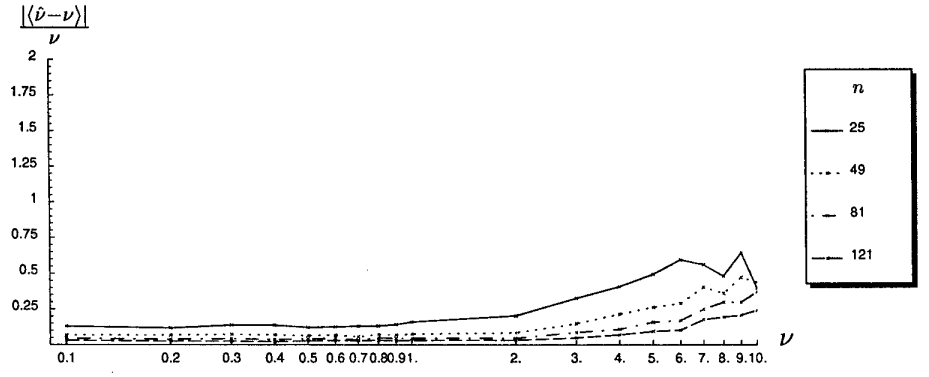

(c) $L = 4$

Figure 29: The absolute value of the relative bias of the estimated order using measure W (54) as it varies with ν computed over 1000 simulations with $\mu = 1$ with sample sizes of 25, 49, 81 121 with looks $L = 1, 2, 4$.

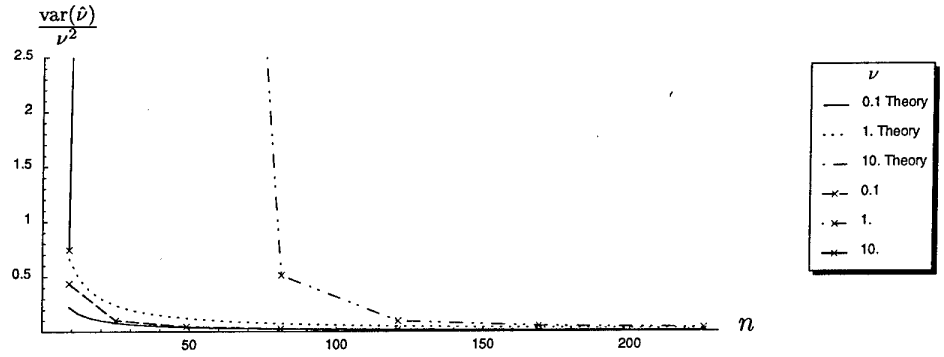

(a) $L = 1$

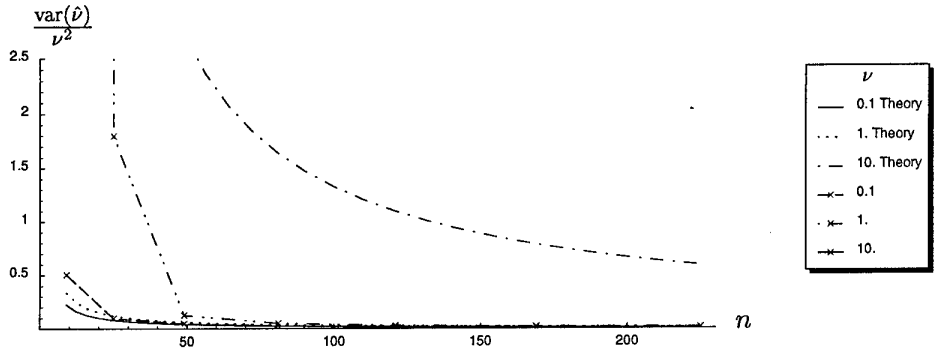

(b) $L = 2$

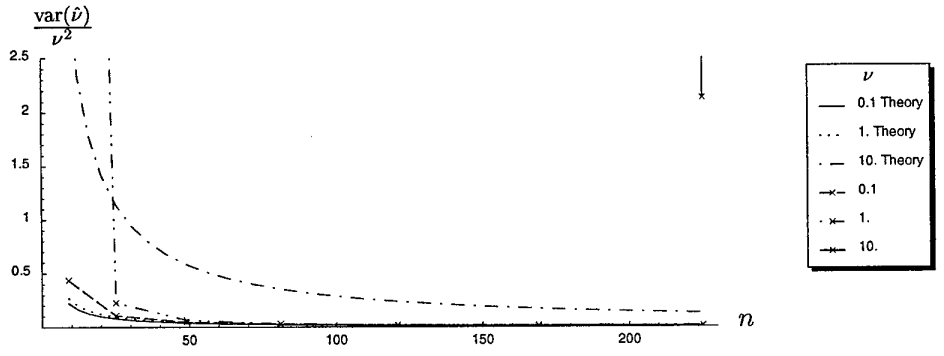

(c) $L = 4$

Figure 30: The normalized variance of the estimated order using measure W (54) as it varies with sample size computed over 1000 simulations with $\mu = 1$. The theoretical (55) and calculated values of the normalized variance of the order estimates are shown for three different values of the order parameter.

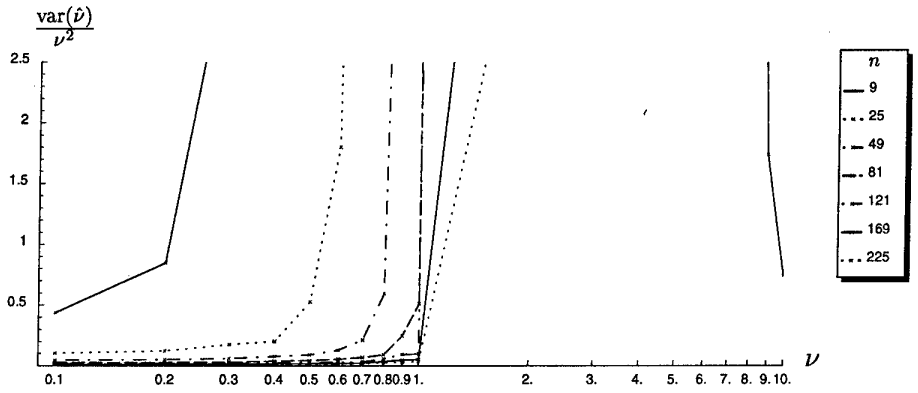

(a) $L = 1$

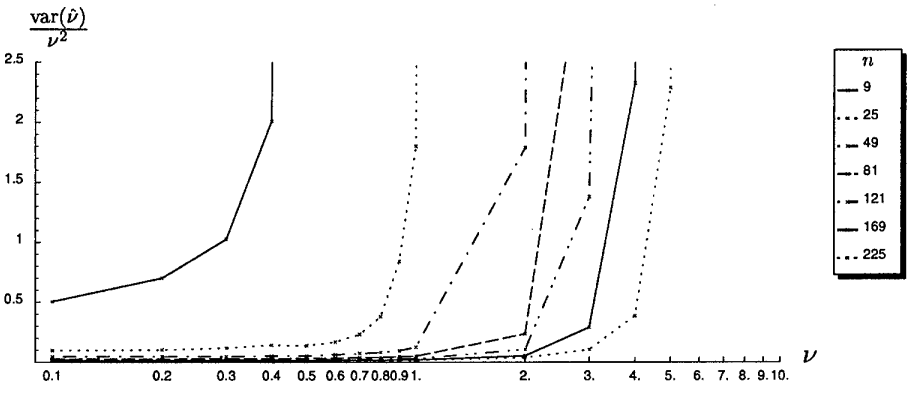

(b) $L = 2$

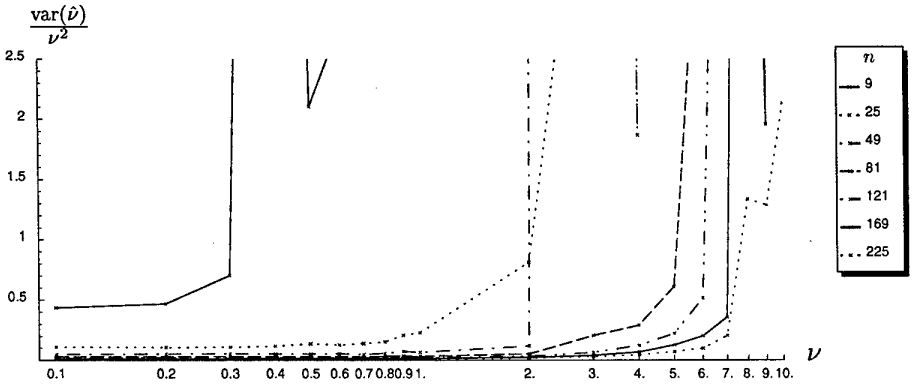

(c) $L = 4$

Figure 31: The normalized variance of the estimated order using measure W (54) as it varies with ν computed over 1000 simulations with $\mu = 1$ for a range of sample sizes and looks $L = 1, 2, 4$.

Blacknell [3] has demonstrated that the sample mean (25) is a good approximation to the maximum likelihood estimate of the mean over a wide rance of parameter values and provides a better performance than (50) using the mean and variance of the logarithm of the data. Comparing figures 9–10 with figures 26–27 confirms the superior performance fo the sample mean. In the later figures, an *a priori* value of ν was used, whereas Blacknell used measure W (54) to compute $\hat{\nu}$ to use in (50), so here the performance of (50) is better than it would be in practical applications where ν would need to be estimated, and the performance difference shown in [3] is more pronounced that that observed here. As can be seen from the normalized variance of estimators of the order parameter plots, the error in the order parameter is always larger than that of either mean estimate, so this error would accumulate to make the variance of the mean estimate from (50) much larger than that indicated in figures 26–27 and indeed larger than that of the sample mean estimate of (25).

Blacknell concludes the minimum normalized variance for the sample mean occurs when the samples are single look ($L = 1$). This seems to be in disagreement with the results presented here where increasing the number of looks has improved the estimates. There is a simple explanation for this. Blacknell and Oliver in their papers have fixed the number of samples available prior to the multi-look averaging whereas in the work reported here n is varied, the number of independent samples after multi-look averaging has taken place. That is, they fix N, the total number of independent samples available from all looks, and samples are averaged in groups of size L to form the L-look sample of size $n = N/L$. The approach of fixing n, the multi-look sample, rather than N is done here because of the band-width limited datalink application at which this work is aimed. In our application, the SAR image formation (including multi-looking) is performed on the aerial platform, and the complete intensity image is then downloaded to be further processed in a ground station over the datalink. Currently, the datalink does not have the capacity to download the individual SAR images that are formed prior to multi-looking. If channel capacity were not a limiting factor, then treating the individual looks separately to obtain more samples is justified. In other words, the improvements in the estimates with an increase in L is less than for the corresponding increase in n for $N = nL$ fixed. We will see that this is true of the order estimates as well.

The estimator in (28) proved to be unreliable in practice (section 5.3). The variation in second order moment estimate term in (28) frequently caused the resulting mean estimate to be negative, and this problem grew in proportion with ν.

To conclude, sample mean of the intensity data with the highest number of looks for a fixed sample size n is the best estimate of μ, the mean parameter of the K distribution.

5.9.2 Order Parameter Estimation

The order parameter estimate has asymptotic Cramer-Rao lower bounds for its variance in the limit of large ν, given by [18]

$$\sigma^2_{\nu,CR} = \frac{\nu^4}{n}. \tag{56}$$

Blacknell [3] has derived an expression for the Fisher information matrix for the K distribution from which the exact Cramer-Rao lower bound can be computed numerically for

the case when the difference between L and ν is an integer. The expressions however are very complicated so I refer the reader to the plots presented by Blacknell [3].

It can be seen from sections 5.2–5.8 that K distribution order parameter estimation consists of two steps: computing a measure, then inversion of a function of that derived measure to give the estimated order parameter. Some situations would not require both stages of the process to be performed — the measure might be sufficient on its own, *e.g.*, segmentation could be done on the measure values directly. We saw that in section 5.4 in the case of Raghavan's method that both steps introduce their own errors, and that these errors change across the range of ν values encountered in practice.

Joughin *et. al* [17] present an analysis based on simulation of the performance of Raghavan's method against two method of moments approach, one using the second and fourth moment (38), and the other the first and second moment (41), against the maximum likelihood approach. (Remember that the maximum likelihood approach requires a two dimensional search in the space defined by the parameters of the likelihood function (24) which is too expensive computationally for our application.) Raghavan's method is shown to be close in its performance to the maximum likelihood method. From this we can infer that using moments of the logarithm of the data would also perform well in estimating the order ν. These issues were examined more thoroughly by Lombardo and Oliver [18] and Blacknell [3] in their consideration of estimators (41), (47) and (54).

When estimating the order parameter ν in the single look case, Blacknell shows that using the texture measure U (mean of logarithm of data) in (47) is better than the variance of logarithm measure W in (54) and the contrast measure V in (41) for a wide range of parameter values. However, for $\nu \geqslant 8.0$, the contrast measure V is the best performer (closest to Cramer-Rao lower bound) when the number of looks is varied under the assumption that N (the total number of independent samples prior to multi-look averaging) is fixed. Comparing figures 19–20 and figures 23–24, measure U is the best for fixed sample size n (the total number of independent samples after multi-look averaging). As in the mean estimate case, improvements in the estimates with an increase in L is less than for the corresponding increase in n for $N = nL$ fixed. Lombardo and Oliver [18] show that in the limit of large ν to first order in $1/\nu$ (assuming n is sufficiently large), the relative variance in estimate $\hat{\nu}$ from the three measures V, U and W is given by

$$
\begin{aligned}
V: \quad & \frac{\mathrm{var}(\hat{\nu})}{\nu^2} \approx \frac{\nu^2}{n}\left(1+\frac{10}{\nu}\right), \\
U: \quad & \frac{\mathrm{var}(\hat{\nu})}{\nu^2} \approx \frac{4\nu^2}{n}\left(\frac{\pi^2}{6}-1+\frac{1}{\nu}\right), \\
W: \quad & \frac{\mathrm{var}(\hat{\nu})}{\nu^2} \approx \frac{\nu^2}{n}\left(\frac{11\pi^2}{90}+\frac{2\pi^2}{3\nu}\left(1-\frac{11\pi^2}{90}\right)\right),
\end{aligned}
$$

in the single look case. It can be seen that the contrast measure V is asymptotically optimal with increasing ν, assuming that n is large enough for the first order approximation to be valid, whereas the other estimators are not indicating that there is still some merit in measure V over U in the limit of large ν and n. When the number of looks is varied while estimating ν for fixed $N = nL$, measure U is the best over all values of ν, and the number of looks at which this occurred was $L = 1$ for $0.1 \leqslant \nu \leqslant 1$ and then $L = \nu$ beyond this (it was computed numerically at integer values of ν beyond $\nu > 1$) [3]. Overall, using measure U for ν with single look data is the clear winner when N is fixed. When n is fixed, U is

still the best measure, and the larger the L the better. Figure 32 shows how measure U is the best of the three, while figure 33 shows that increasing the number of looks does improve the estimate of the order for fixed n. Figures 34 and 35 show the same things for the relative bias.

The Cramer-Rao lower bound in (56) for large ν indicates that to maintain constant error in the estimate of the order parameter, the number of samples should be proportional to the square of the order parameter. The consequence of this is that with fixed values of n, a value of ν is rapidly attained beyond which the estimate is meaningless [18]. Under realistic conditions with a small number of samples the statistical uncertainty in the data will occasionally lead to non-invertible results, *e.g.*, a realization of contrast measure having value less than one. As discussed previously, I have interpreted such results as the measure indicating the presence of a constant radar cross-section [28].

Lombardo and Oliver [18] show that at least in the case of the contrast measure V, the bias and variance of the measure (before inversion to determine the estimate $\hat{\nu}$) is well represented by theory. However, a first order expansion for the inversion process from the measures to give the bias of the resulting estimates $\hat{\nu}$ given in (42) and (48) is not sufficient to account for the nonlinearity of this inversion. They therefore derive the following improved approximation to the bias in the single look case,

$$
\begin{aligned}
V: \quad & \langle \hat{\nu} - \nu \rangle = \frac{\nu^2}{n}\left[(1+\frac{1}{\nu})(1+\frac{6}{\nu}) + \nu(1+\frac{1}{\nu})(1+\frac{4}{\nu})(1+\frac{5}{\nu})\right] \\
U: \quad & \langle \hat{\nu} - \nu \rangle = \frac{\nu}{2n(\nu\psi^{(1)}(\nu)-1)}\left[1+\frac{2}{\nu} - \frac{\psi^{(2)}(\nu)+\frac{1}{\nu^2}}{2(\nu\psi^{(1)}(\nu)-1)^2}\left(\psi^{(1)}(\nu)+\frac{\pi^2}{6}-1\right)\right] \qquad (57) \\
W: \quad & \langle \hat{\nu} - \nu \rangle = -\frac{\nu}{n\nu\psi^{(2)}(\nu)}\left[\psi^{(1)}(\nu)+\frac{\pi^2}{6} + \right. \\
& \left. \frac{\psi^{(3)}(\nu)}{2(\nu\psi^{(2)}(\nu))^2}\left(\psi^{(3)}(\nu) + 2\left(\psi^{(1)}(\nu)\right)^2 + \frac{11\pi^4}{90} + \frac{2\pi^2}{3}\psi^{(1)}(\nu)\right)\right]
\end{aligned}
$$

by using a second order Taylor series expansion of each measure about its mean. (Figure 36 indicates that at least for small samples size of $n = 49$ the predicted relative bias (57) is a poor match to measured behaviour.) For large values of ν, Lombardo and Oliver report that there is still a mismatch between the predicted and measured order parameter estimate's normalized variance for which it does not account because it is unable to improve upon the predicted normalized variances (43), (49) and (55) already presented. Therefore knowledge of higher moments than second order of the texture measures V, U and W is required for accurate error prediction, ruling out the possibility of ever doing it for small n (see [30, p. 113]). Furthermore, the estimate $\hat{\nu}$ is much more biased than the texture measures V, U, and W from which it was computed.

Lombardo and Oliver point out that all three measures are proportional to $1/\nu$ for large ν. Therefore, they propose estimating the reciprocal $t \equiv 1/\nu$ instead of ν directly to address the problems mentioned above. Furthermore, because $1/\nu$ is the variance of the underlying gamma distributed cross section in the unit mean case ($\mu = 1$) (1) it could be argued that this is really the parameter of greater interest. In addition, it is intuitive that the mean and variance of the estimate t should go to zero as the texture contrast is

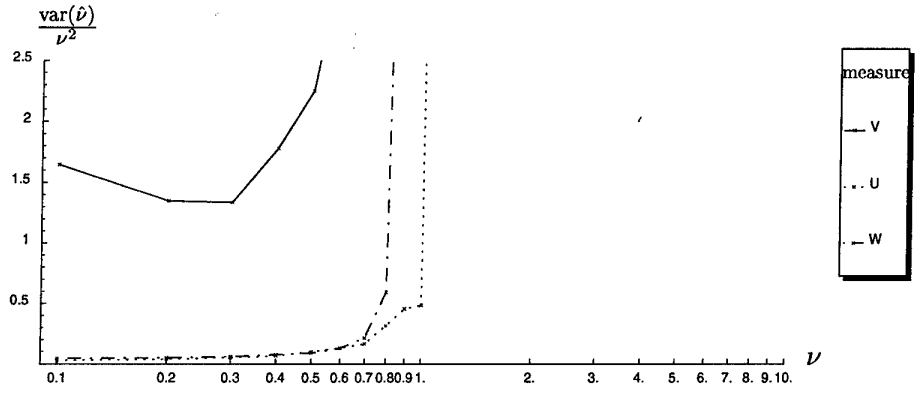

(a) $L = 1$

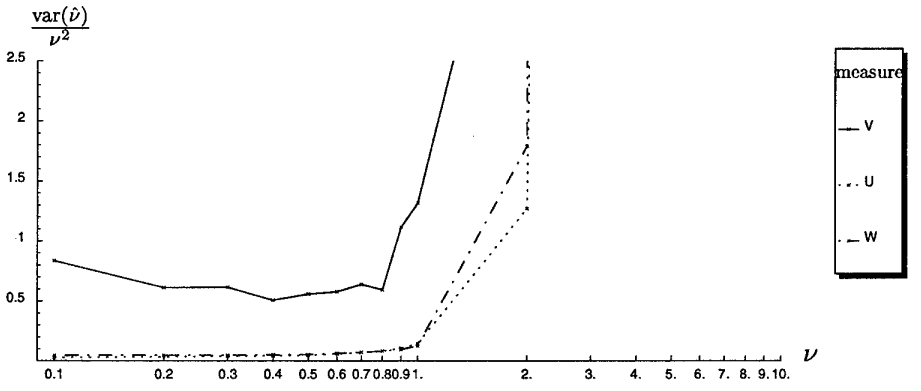

(b) $L = 2$

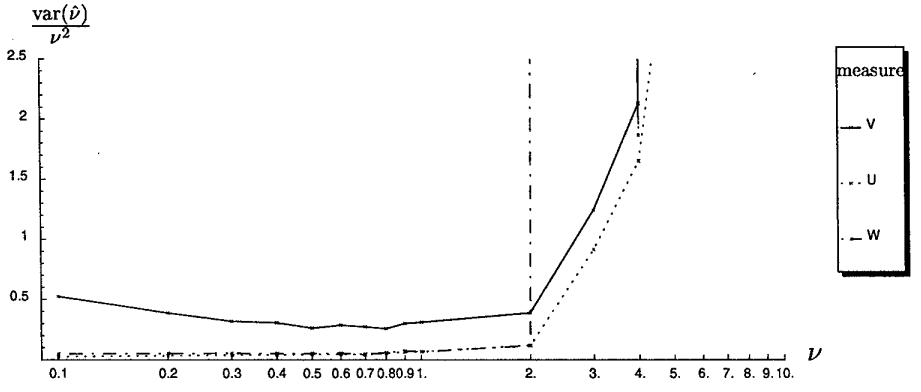

(c) $L = 4$

Figure 32: The normalized variance of the estimated order ν as it varies with ν computed over 1000 simulations with $\mu = 1$ in the cases of $L = 1, 2, 4$. All estimates were computed using 49 samples. The estimates shown here are computed using the measures V (solid line), U (dotted line) and W (dot-dashed line).

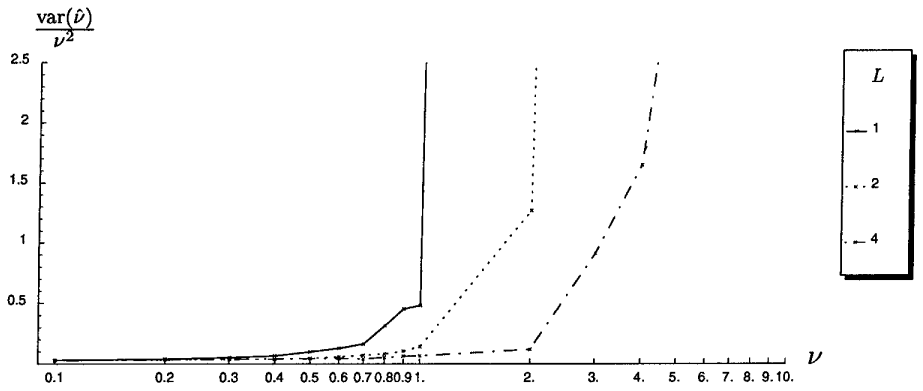

Figure 33: The normalized variance of the estimated order using U as it varies with ν computed over 1000 simulations with $\mu = 1$ in the cases of $L = 1, 2, 4$. All estimates were computed using 49 samples.

reduced (*i.e.* as $\nu \to \infty$). Finally, remember that the probability density function of the K distribution becomes increasingly insensitive to ν as ν increases (figure 1).

The bias of the new estimate $\hat{t}$ can be obtained from the expressions for estimate $\hat{\nu}$ by

$$\frac{\langle \hat{t} - t \rangle}{t} = -\frac{\langle \hat{\nu} - \nu \rangle}{\nu},$$

i.e. by reversing the sign of the bias and substituting $t \equiv 1/\nu$, and the variance of $\hat{t}$ by

$$\frac{\mathrm{var}(\hat{t})}{t^2} = \frac{\mathrm{var}(\hat{\nu})}{\nu^2}.$$

However, in this case there is no need to correct for the nonlinearity of the inversion process. Figure 37 plots the normalized variance of the estimate $\hat{t}$ against the order parameter using the U measure. As expected, the region of higher uncertainty in the estimate $\hat{t}$ now occurs when ν is small ($\nu < 1.0$). However, for reasonable sample sizes ($n \geqslant 49$), the normalized variance of $\hat{t}$ is better behaved in this region then the normalized variance of $\hat{\nu}$ for $\nu > 1.0$. Finally, Oliver indicated that performance of order parameter estimates is improved if the samples are normalized by their means [27].

5.9.3 Effect of Noise Upon Order Parameter Estimation

Lombardo, Oliver and Tough [19] showed that the normalized logarithm measure U is extremely sensitive to small amounts of noise. They show that in the single look case, the change in the value of U with the addition of noise is approximately

$$e_U \approx s^{-\nu} \left(\frac{1}{\nu} + \gamma + \log \nu \right) \tag{58}$$

where γ is the Euler constant, s is the signal-to-noise ratio (SNR) given by μ/a where a is the variance of the noise (uncorrelated zero-mean Gaussian distributed), and $\nu \ll 1$.

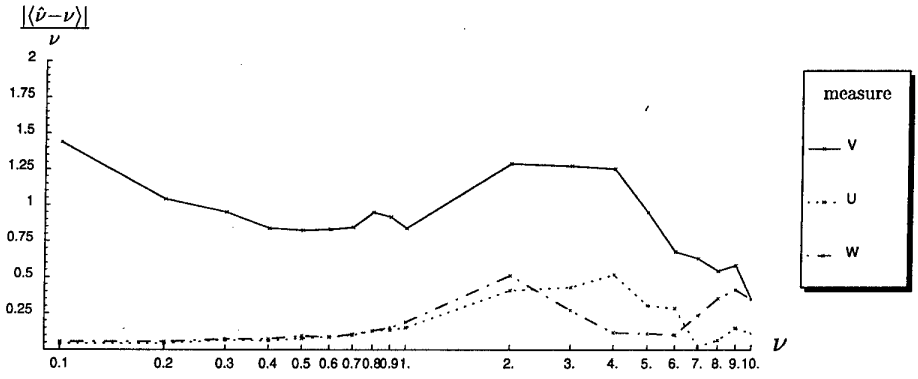

(a) $L = 1$

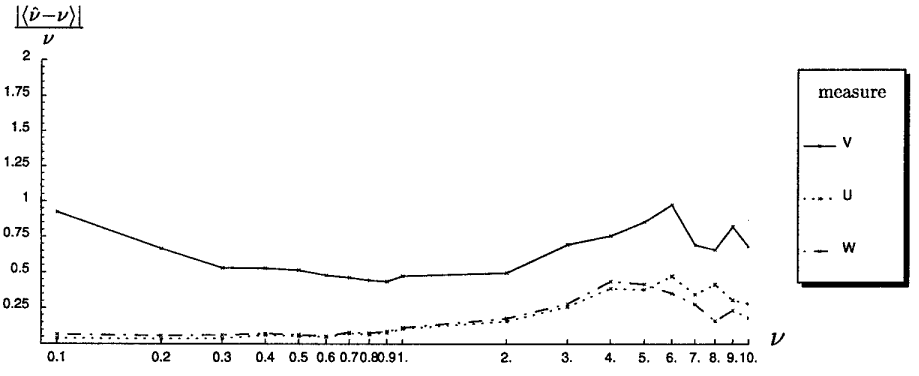

(b) $L = 2$

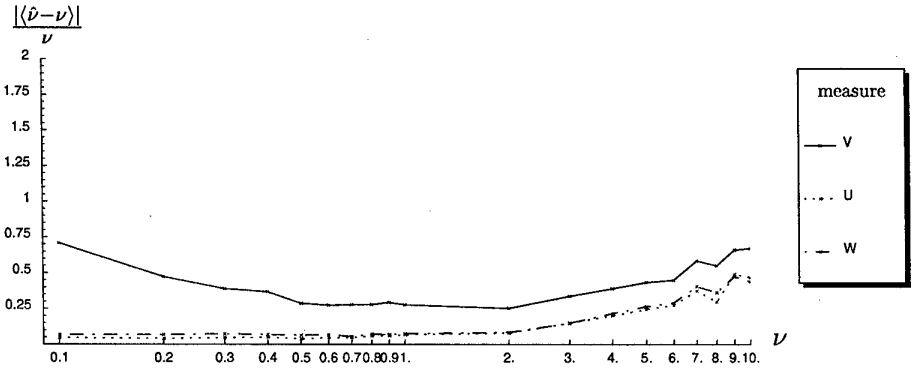

(c) $L = 4$

Figure 34: The absolute value of the relative bias of order estimated using measures V, U and W as it varies with ν computed over 1000 simulations with $\mu = 1$ for a fixed sample size of $n = 49$ for $L = 1, 2, 4$.

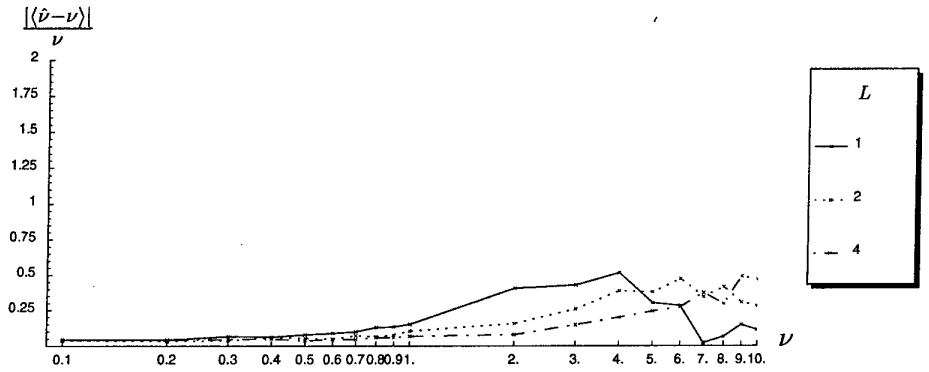

Figure 35: The absolute value of the relative bias of the estimated order using measure U in the $L = 1, 2, 4$ look cases as it varies with ν computed over 1000 simulations with $\mu = 1$ with a sample size of $n = 49$.

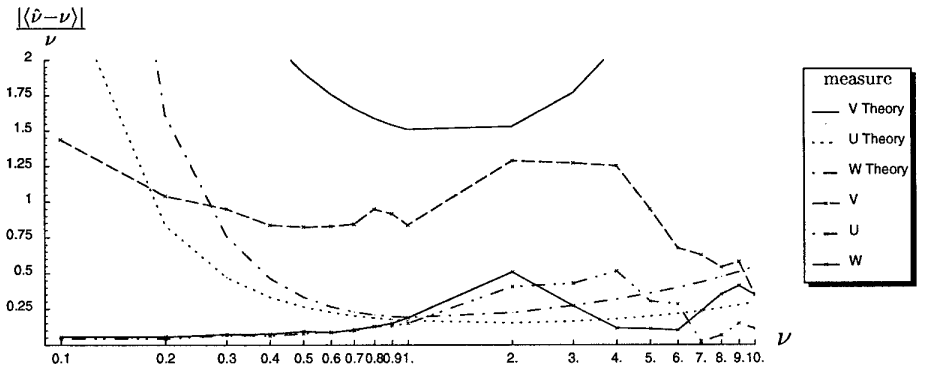

Figure 36: The relative bias of the estimated order parameter (using measures V, U and W) as it varies with ν computed over 1000 simulations with $\mu = 1$ in the single look case plotted against the predicted relative bias from (57). The estimates were all computed using 49 samples.

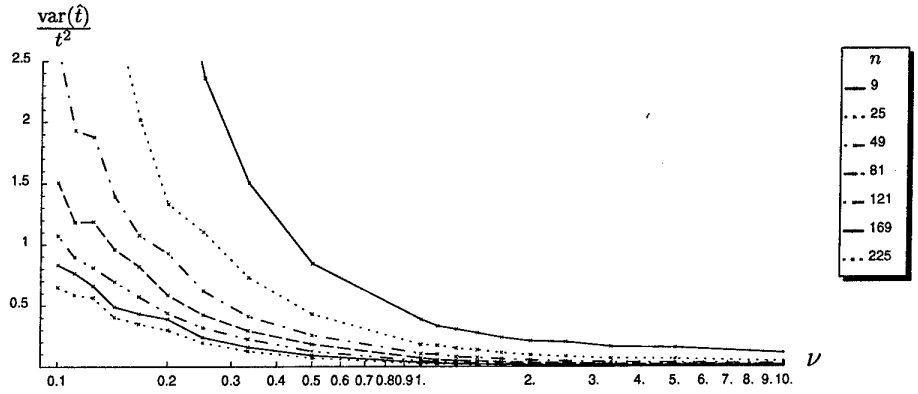

(a) $L = 1$

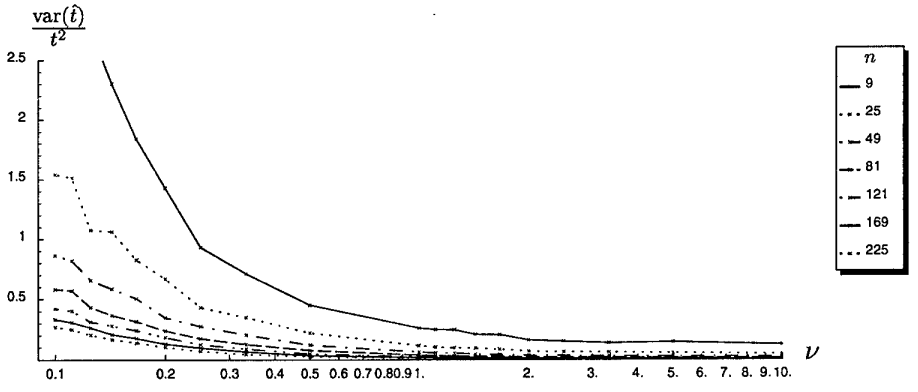

(b) $L = 2$

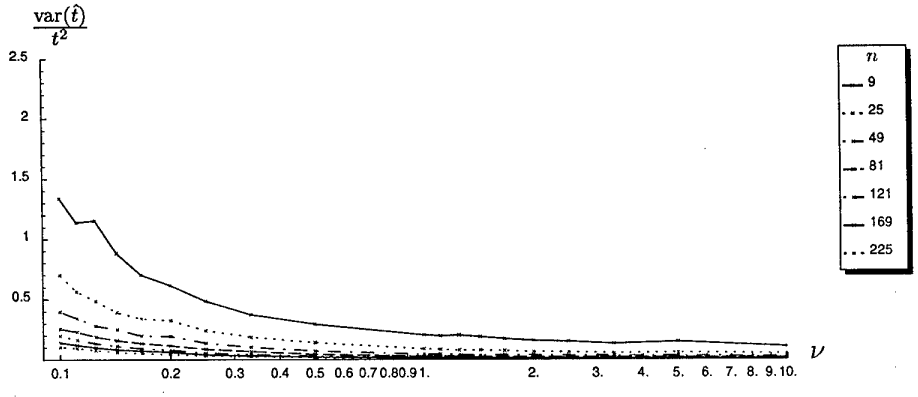

(c) $L = 4$

Figure 37: The normalized variance of the estimate $\hat{t}$ using measure U as it varies with ν computed over 1000 simulations with $\mu = 1$ for a range of sample sizes for $L = 1, 2, 4$.

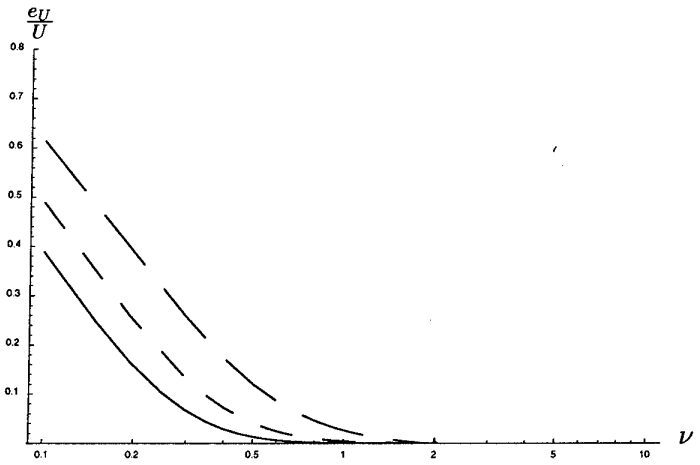

Figure 38: Plot of the normalized change in the value of U that results from the addition of noise (59) as a function of ν for the cases of SNR of 20 dB (long dashes), 30 dB (short dashes) and 40 dB (solid line).

This equation is highly nonlinear, and for example with $\nu = 0.1$ a SNR of 300 dB would be required for a fractional bias of 0.01, although for larger ν the required SNR is more reasonable. The full expression for the change in U is given by

$$e_U = \frac{1}{\Gamma(\nu)} \frac{\pi}{\sin \pi\nu} \left\{ \sum_{r=0}^{\infty} \frac{\left(\frac{\nu}{s}\right)^{r+\nu}}{(r+\nu)r!} - \frac{\left(\frac{\nu}{s}\right)^{r+1}}{(r+\nu)\Gamma(r+2-\nu)} \right\} - \log(1+\frac{1}{s}), \tag{59}$$

which is depicted in figure 38. They demonstrate that the contrast measure V is more robust to noise, because the fractional increase in V is approximately $2/s$ for large s. Therefore its systematic error is not significant compared to the bias due to small sample sizes. However its utility is limited because of its relative insensitivity to variations in the order parameter — the measure V has a large normalized variance when compared to that of the U measure.

As a consequence, Lombardo *et al.* [19] proposed a new measure based on the contrast of the square root of intensity (*i.e.* amplitude) that is a compromise between the two. The new *amplitude contrast* measure V_a is defined by

$$V_a \equiv \frac{\langle x_i \rangle - \langle \sqrt{x_i} \rangle^2}{\langle \sqrt{x_i} \rangle^2}. \tag{60}$$

Then from the probability density function of the K distribution (4), the estimate $\hat{\nu}$ can be obtained by solving

$$V_a = \frac{L\nu\Gamma(L)^2\Gamma(\nu)^2}{\Gamma(L+1/2)^2\Gamma(\nu+1/2)^2} - 1. \tag{61}$$

They show through simulation that this measure is much less sensitive to noise than the normalized log estimator U, *i.e.* its bias is smaller, but not as insensitive as the contrast

estimator V. Likewise, its variance lies between that of U and V, so its sensitivity to the order parameter is also a compromise between the two. If however, one is only interested in distinguishing between one region and another (*e.g.*, a target from its background) then the problems associated with noise producing a bias in the normalized logarithm measure is not important because the bias is a monotonic function of ν and the SNR, and the normalized variance of U is almost insensitive to noise as V_a, whereas the normalized variance of the amplitude contrast measure V_a is greater than that of U. Therefore one should adopt the amplitude contrast measure for texture segmentation only when noise is high — otherwise the normalized log measure should be used.

5.9.4 A Combined Estimator for the Order Parameter

Lombardo, Oliver and Tough [19] show that the triple of sample mean $\hat{\mu}$ and the measures U and V form an approximate sufficient statistic for independent K distributed random variables, being exact for an approximation to the K distribution for the case of large L. This is reasonable given that U is a good measure for deriving the order in cases when $\nu < 8.0$, and V in the cases where $\nu \geqslant 8.0$ according to [3]. Consequently, these three statistics should form the basis of a feature vector to discriminate different textured regions of a SAR image. This motivates the modified estimator of Jahangir, Blacknell and White [12], which is defined to be a linear combination of normalized logarithm of intensity measure U and the contrast of the amplitude V_a,

$$\begin{aligned} M &\equiv \alpha U + (1-\alpha)V_a \\ &= \alpha(\langle \log x_i \rangle - \log \langle x_i \rangle) + (1-\alpha)\left(\frac{\langle x_i \rangle - \langle \sqrt{x_i} \rangle^2}{\langle \sqrt{x_i} \rangle^2}\right) \end{aligned} \tag{62}$$

where $\alpha = 0.8$ was found to be the best compromise. From the moments of the K distribution,

$$M = \alpha\left(\log\hat{\nu} - \psi^{(0)}(\hat{\nu}) + \log L - \psi^{(0)}(L)\right) + (1-\alpha)\left(\frac{L\nu\Gamma(L)^2\Gamma(\nu)^2}{\Gamma(L+1/2)^2\Gamma(\nu+1/2)^2} - 1\right) \tag{63}$$

which is solved for ν. The predicted variance of t for the new measure in the single look case to first order in $1/n$ can be found in (9) of [12]. The performance of this measure was shown to agree closely with the predicted value from (9) of [12] and to be indistinguishable from the maximum likelihood result over a wide range of $t > 0.5$. Simulation results are presented in figure 39 and comparison with figure 37 indicates that the performance improvement, if any, over measure U alone is hard to discern and so the additional complexity does not seem warranted.

5.10 Recommendations

Let us now summarize the discussion so far on parameter estimation for the K distribution. Firstly, the mean parameter is best estimated using the sample mean. In datalink bandwidth-limited applications where multi-looking is performed prior to transmission,

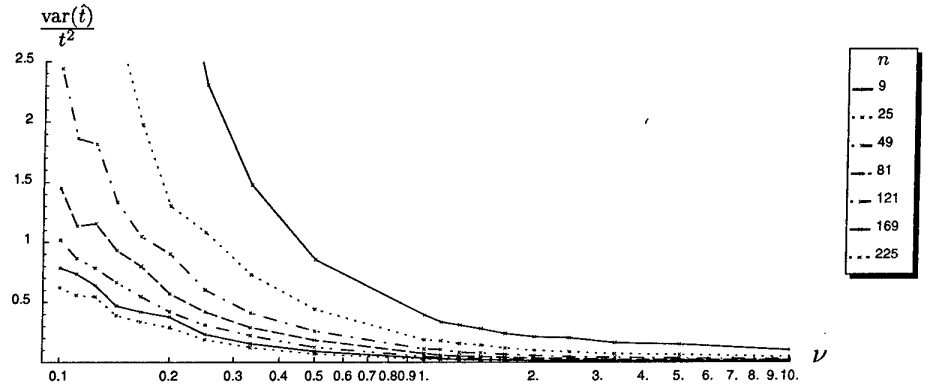

(a) $L = 1$

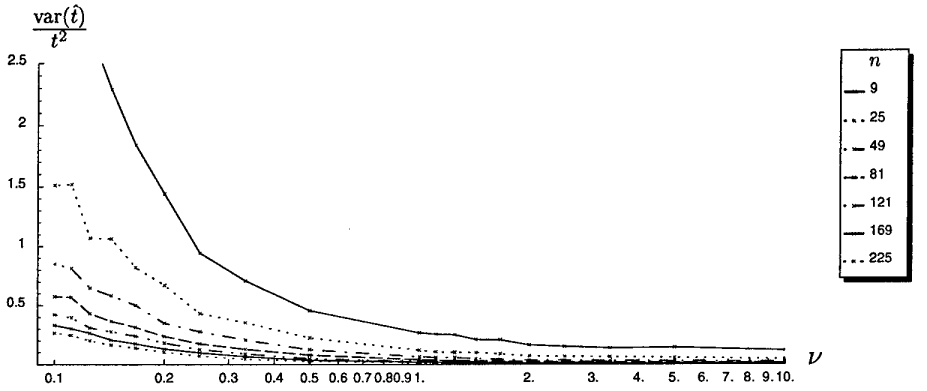

(b) $L = 2$

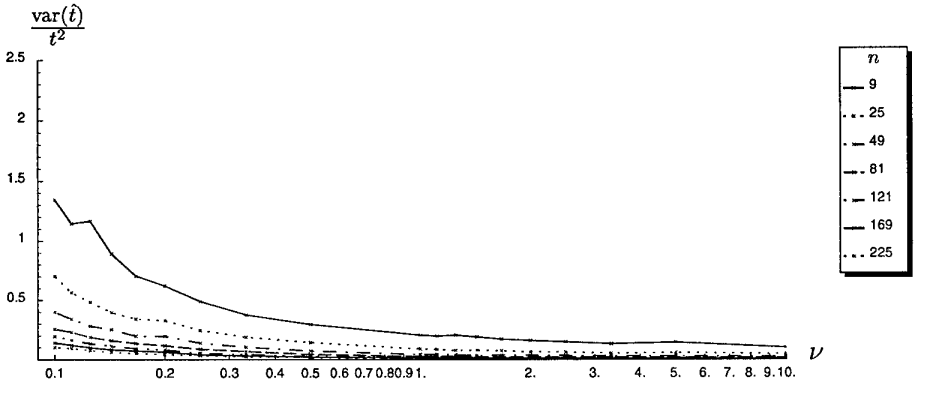

(c) $L = 4$

Figure 39: The normalized variance of the estimate $\hat{t}$ using measure M (63) as it varies with ν computed over 1000 simulations with $\mu = 1$ for a range of sample sizes and $L = 1, 2, 4$.

imagery averaged across as many looks as possible is best. When there is no such limitation, it is best to treat the looks individually and have the corresponding increase in sample size. This behaviour is true of order parameter estimation as well.

Next, before estimating the order parameter, the samples should be normalized by the mean estimate. The normalized logarithm of intensity measure U is the best measure from which to compute the order parameter estimate. Where possible, it is better to use the parameter $t \equiv 1/\nu$ rather than ν to characterize a sample because of its smaller variance. This might be appropriate in many classification applications. Furthermore, it may be sufficient to simply use the value of the measure U as a feature for classification and save the work of the inversion process in some applications. The fact that V and U form a sufficient statistic for the K distribution in the limit of large L suggests that using both as part of a feature vector for classification may give improved performance over using U alone.

6 Effect of Correlation Upon Estimators

The results presented so far on the variance of the estimators for the parameters of the K distribution assume that the samples are uncorrelated. When the samples are correlated, the variance of the estimates will be larger than is indicated by the same number of samples for an uncorrelated case. Consequently, more samples are required in the correlated case than the uncorrelated case to achieve the same variance on the estimators. We can see this from the following discussion for the estimate of the mean [33,34].

Let $\mathbf{X} = (\mathbf{x}_1, \ldots, \mathbf{x}_n)$ denote the vector of random variables that correspond to the random sample (in lexicographic order if the sample is taken from a random field). Next, let $\mathbf{C}$ denote the covariance matrix. Furthermore, let us assume that the sample is from a stationary spatial process, *i.e.* the correlation between two random variables $\mathbf{x}_i$ and $\mathbf{x}_j$ is dependent on only the spatial displacement between i and j. If the spatial process of the sample $\mathbf{X}$ is one-dimensional, $\mathbf{C}$ is a symmetric Toeplitz matrix because $[\mathbf{C}]_{ij} = \sigma^2 \rho_{\mathbf{X}}(|i-j|)$, where $\rho_{\mathbf{X}}(s)$ is the correlation at lag s and σ^2 is the variance of each $\mathbf{x}_i$. When the spatial process of $\mathbf{X}$ is two-dimensional of size $p \times q$ (*i.e.* , $n = pq$), then $\mathbf{C}$ is symmetric block Toeplitz with Toeplitz blocks, *i.e.* $[\mathbf{C}]_{ij,kl} = \sigma^2 \rho_{\mathbf{X}}(i-k, j-l)$ where the paired indices ij and kl denote lexicographic order and $i, k = 1, \ldots, p$ and $j, l = 1, \ldots, q$. Then the variance on the estimate $\hat{\mu}$ of the mean μ, is given by

$$\mathrm{var}(\hat{\mu}) = \frac{\sigma^2}{n} \sum_{s=-n+1}^{n-1} (1 - \frac{|s|}{n}) \rho_{\mathbf{X}}(s)$$

in the case of a one-dimensional spatial process, and

$$\mathrm{var}(\hat{\mu}) = \frac{\sigma^2}{n} \sum_{s=-q+1}^{q-1} \sum_{r=-p+1}^{p-1} (1 - \frac{|r||s|}{pq}) \rho_{\mathbf{X}}(r, s)$$

in the case of a two-dimensional spatial process. Similar results can be obtained for the variance of the population variance estimator [33, p. 144].

Consequently, it can be seen that the variance of the mean estimator is increased by the correlation at non-zero lags, weighted by the length of each lag. Methods exist to estimate $\text{var}(\hat{\mu})$ that take correlation into account [21].

7 Conclusion

This paper has reviewed a number of different moment-based methods for estimating the parameters of the K distribution. The K distribution is a model for the statistics of SAR imagery that is formed from the product of two independent distributions, one representing the radar cross-section, and the other representing speckle that is a characteristic of coherent imaging. A method for synthesizing correlated K-distributed random fields has been reviewed. Moments of intensity, log intensity and amplitude statistics were used to compute measures which are inverted to give estimates of the mean and order parameters of the K distribution. A method based on the normalized logarithm of intensity was shown to give the best performance, confirming the results of Oliver (1993) and Blacknell (1994). The effect of correlation upon order parameter estimation and its role in the K distribution's underlying component pertaining to the radar cross-section was briefly reviewed.

8 Bibliography

[1] M. Abramowitz and I. A. Stegun, Handbook of Mathematical Functions. New York, Dover, 1968.

[2] B. C. Armstrong and H. D. Griffiths, "Modelling spatially correlated K-distributed clutter," Electronic Letters, **27**, no. 15, pp. 1355–1356, 1991.

[3] D. Blacknell, "Comparison of parameter estimators for K-distribution," IEE Proceedings, Radar, Sonar and Navigation, **141**, no. 1, pp. 45–52, 1994.

[4] D. Blacknell, A. Blake, P. Lombardo and C. J. Oliver, "A comparison of simulation techniques for correlated gamma and K-distributed images for SAR applications," International Geoscience and Remote Sensing Symposium, Pasadena, California USA, pp. IV 2182–2184, Aug., 1994.

[5] A. P. Blake, D. Blacknell and C. J. Oliver, "Texture simulation and analysis in coherent imagery," Fifth International Conference on Image Processing and its Applications, pp. 772–776, 4-6 July, 1995.

[6] P. B. Chapple, D. C. Bertilone, R. S. Caprari and G. N. Newsam, "Stochastic model-based processing for detection of small targets in non-Gaussian natural imagery," in preparation, 1998.

[7] C. R. Dietrich and G. N. Newsam, "A fast and exact method for multidimensional Gaussian stochastic simulations," Water Resources Research, **29**, no. 8, pp. 2861–2869, 1993.

[8] C. R. Dietrich and G. N. Newsam, "Fast and exact simulation of stationary Gaussian processes through circulant embedding of the covariance matrix," SIAM Journal of Scientific Computing, **18**, no. 4, pp. 1088–1107, 1997.

[9] J. R. Garside and C. J. Oliver, "Models for natural clutter in coherent imaging," SPIE Conference on Image Processing III, **1135**, pp. 48–55, 1989.

[10] I. S. Gradshteyn and I. M. Ryzhik, Table of Integrals Series and Products. London, Academic Press, 1965.

[11] C. W. Helstrom, Probability and Stochastic Processes for Engineers (second edition). New York, Macmillan Publishing Company, 1991.

[12] M. Jahangir, D. Blacknell and R. G. White, "Accurate approximation to the optimum parameter estimate for K-distributed clutter," IEE Proceedings, Radar, Sonar and Navigation, **143**, no. 6, pp. 383–390, 1996.

[13] E. Jakeman and P. N. Pusey, "A model for non-Rayleigh sea echo," IEEE Transactions on Antennas and Propagation, **24**, no. 6, pp. 806–814, 1976.

[14] E. Jakeman and P. N. Pusey, "Significance of K distributions in scattering experiments," Physical Review Letters, **40**, no. 9, pp. 546–550, 1978.

[15] E. Jakeman, "On the statistics of K-distributed noise," Journal of Physics A: Mathematics and General, **13**, pp. 31–48, 1980.

[16] E. Jakeman and R. J. A. Tough, "Generalized K distribution: a statistical model for weak scattering," Journal of the Optical Society of America A, **4**, no. 9, pp. 1764–1772, 1987.

[17] I. R. Joughin, D. B. Percival and D. P. Winebrenner, "Maximum likelihood estimation of K distribution parameters for SAR data," IEEE Transactions on Geoscience and Remote Sensing, **31**, no. 5, pp. 989–999, 1993.

[18] P. Lombardo and C. J. Oliver, "Estimation of texture parameters in K-distributed clutter," IEE Proceedings on Radar, Sonar and Navigation, **141**, pp. 196–204, 1994.

[19] P. Lombardo, C. J. Oliver and R. J. A. Tough, "Effect of noise on order parameter estimation for K-distributed clutter," IEE Proceedings, Radar, Sonar and Navigation, **142**, no. 1, pp. 33–40, 1995.

[20] P. Lombardo and C. J. Oliver, "Estimating the correlation properties of K-distributed SAR clutter," IEE Proceedings, Radar, Sonar and Navigation, **142**, no. 4, pp. 167–178, 1995.

[21] P. A. P. Moran, "The estimation of standard errors in Monte Carlo simulation experiments," Biometrika, **62**, pp. 1–4, 1975.

[22] C. J. Oliver, "A model for non-Rayleigh scattering statistics," Optica Acta, **31**, no. 6, pp. 701–722, 1984.

[23] C. J. Oliver, "Correlated K-distributed clutter models," Optica Acta, **32**, no. 12, pp. 1515–1547, 1985.

[24] C. J. Oliver and R. J. A. Tough, "On the simulation of correlated K-distributed random clutter," Optica Acta, **33**, no. 3, pp. 223–250, 1986.

[25] C. J. Oliver, "The interpretation and simulation of clutter textures in coherent images," Inverse Problems, **2**, pp. 481–518, 1986.

[26] C. J. Oliver, "The sensitivity of texture measures for correlated random clutter," Inverse Problems, **5**, pp. 875–901, 1989.

[27] C. J. Oliver, "Optimum texture estimators for SAR clutter," Journal of Physics D: Applied Physics, **26**, pp. 1824–1835, 1993.

[28] C. J. Oliver and S. Quegan, Understanding synthetic aperture radar images. Norwood, MA, Artech House, 1998.

[29] C. J. Oliver, A. Blake and R. G. White, "Optimum texture analysis of synthetic aperture radar images," SPIE Proceedings, Algorithms for Synthetic Aperture Radar Imagery, **2230**, pp. 389–398, Apr., 1994.

[30] A. Papoulis, Probability, Random Variables, and Stochastic Processes (third edition). New York, McGraw-Hill, 1991.

[31] R. S. Raghavan, "A model for spatially correlated radar clutter," IEEE Transactions on Aerospace and Electronic Systems, **27**, no. 2, pp. 268–275, 1991.

[32] R. S. Raghavan, "A method for estimating parameters of K-distributed clutter," IEEE Transactions on Aerospace and Electronic Systems, **27**, no. 2, pp. 238–246, 1991.

[33] B. D. Ripley, Stochastic Simulation. New York, John Wiley & Sons, 1987.

[34] C. W. Therrien, Discrete Random Signals and Statistical Signal Processing. Englewood Cliffs, NJ, Prentice Hall, 1992.

[35] K. D. Ward, "Compound representation of high resolution sea clutter," Electronic Letters, **17**, no. 6, pp. 561–563, 1981.

[36] D. Zwillinger, Ed., CRC Standard Mathematical Tables and Formulae (thirtieth edition): Boca Raton, 1996.

DISTRIBUTION LIST

Estimating the Parameters of the K Distribution in the Intensity Domain

Nicholas J. Redding

	Number of Copies
DEFENCE ORGANISATION	
Task Sponsor	
DD JP129, DG Aerospace Division	1
S&T Program	
Chief Defence Scientist FAS Science Policy AS Science Corporate Management	1
Director General Science Policy Development	1
Counsellor, Defence Science, London	Doc Data Sht
Counsellor, Defence Science, Washington	Doc Data Sht
Scientific Adviser Policy and Command	1
Navy Scientific Adviser	Doc Data Sht
Scientific Adviser, Army	1
Air Force Scientific Adviser	1
Director Trials	1
Aeronautical and Maritime Research Laboratory	
Director, Aeronautical and Maritime Research Laboratory	1
Electronics and Surveillance Research Laboratory	
Director, Electronics and Surveillance Research Laboratory	1
Chief, Surveillance Systems Division	1
Research Leader, Imagery Systems	1
Head, Image Analysis & Exploitation	1
Dr Irina Antipov	1
Dr Brett Haywood	1
Dr Bridget Hobbs	1
David I. Kettler	1
Dr Graeme Nash	1
Dr Garry Newsam	1
Dr Nicholas J. Redding	4
Brian Reid	1
Rodney Smith	1
Dr Nick J. S. Stacy	1

Kathleen Zyga	1
DSTO Libraries	
Library Fishermens Bend	1
Library Maribyrnong	1
Library Salisbury	2
Australian Archives	1
Library, MOD, Pyrmont	Doc Data Sht
Capability Development Division	
Director General Maritime Development	Doc Data Sht
Director General Land Development	1
Director General C3I Development	Doc Data Sht
Director General Aerospace Development	1
Navy	
SO(Science), Director of Naval Warfare, Maritime Headquarters Annex, Garden Island	Doc Data Sht
Intelligence Program	
DGSTA Defence Intelligence Organisation	1
Acquisition Program	
JP129 Program Manager	1
Corporater Support Program(libraries)	
Officer in Charge, TRS, Defence Regional Library, Canberra	1
Additional copies for DEC for exchange agreements	
US Defense Technical Information Center	2
UK Defence Research Information Centre	2
Canada Defence Scientific Information Service	1
NZ Defence Information Centre	1
SPARES	
DSTO Salisbury Research Library	6
Total number of copies:	48

DEFENCE SCIENCE AND TECHNOLOGY ORGANISATION DOCUMENT CONTROL DATA				1. CAVEAT/PRIVACY MARKING
2. TITLE Estimating the Parameters of the K Distribution in the Intensity Domain			3. SECURITY CLASSIFICATION Document (U) Title (U) Abstract (U)	
4. AUTHOR(S) Nicholas J. Redding			5. CORPORATE AUTHOR Electronics and Surveillance Research Laboratory PO Box 1500 Salisbury, South Australia, Australia 5108	
6a. DSTO NUMBER DSTO–TR–0839	6b. AR NUMBER 011-015		6c. TYPE OF REPORT Technical Report	7. DOCUMENT DATE July, 1999
8. FILE NUMBER B9505-17-115	9. TASK NUMBER ARM 97/261	10. SPONSOR DGAD	11. No OF PAGES 60	12. No OF REFS 36
13. DOWNGRADING / DELIMITING INSTRUCTIONS Not Applicable			14. RELEASE AUTHORITY Chief, Surveillance Systems Division	

15. SECONDARY RELEASE STATEMENT OF THIS DOCUMENT

Approved For Public Release

OVERSEAS ENQUIRIES OUTSIDE STATED LIMITATIONS SHOULD BE REFERRED THROUGH DOCUMENT EXCHANGE CENTRE, DIS NETWORK OFFICE, DEPT OF DEFENCE, CAMPBELL PARK OFFICES, CANBERRA, ACT 2600

16. DELIBERATE ANNOUNCEMENT

No Limitations

17. CITATION IN OTHER DOCUMENTS

No Limitations

18. DEFTEST DESCRIPTORS

synthetic aperture radar
image analysis
air surveillance

19. ABSTRACT

This paper reviews a number of different moment-based methods for estimating the parameters of the K distribution. The K distribution is a model for the statistics of synthetic aperture radar (SAR) imagery that is formed from the product of two independent distributions, one representing the radar cross-section, and the other representing speckle that is a characteristic of coherent imaging. A method for synthesizing correlated K-distributed random fields is reviewed. Moments of intensity, log intensity and amplitude statistics are used to compute measures which are inverted to give estimates of the mean and order parameters of the K distribution. A method based on the normalized logarithm of intensity is shown to give the best performance, confirming the results of Oliver (1993) and Blacknell (1994). The effect of correlation upon order parameter estimation and its role in the K distribution's underlying component pertaining to the radar cross-section is briefly considered. This work will be used to development target detection algorithms to find targets of interest in SAR imagery.